Impacts of meteorological nudging on the global dust cycle simulated by NICAM coupled with an aerosol model

Article · July 2018

DOI: 10.1016/j.atmosenv.2018.07.016

8 authors, including:

T. Dai
Chinese Academy of Sciences

Peng Zhang
China Meteorological Administration

Miho Sekiguchi
Tokyo University of Marine Science and Technology

Kentaroh Suzuki
The University of Tokyo

Atmospheric Environment 190 (2018) 99–115

Contents lists available at ScienceDirect

Atmospheric Environment

journal homepage: www.elsevier.com/locate/atmosenv

Impacts of meteorological nudging on the global dust cycle simulated by NICAM coupled with an aerosol model

Tie Dai[a,b,c,*], Yueming Cheng[b], Peng Zhang[d], Guangyu Shi[a,c], Miho Sekiguchi[e], Kentaroh Suzuki[f], Daisuke Goto[g], Teruyuki Nakajima[h]

[a] State Key Laboratory of Numerical Modeling for Atmospheric Sciences and Geophysical Fluid Dynamics, Institute of Atmospheric Physics, Chinese Academy of Sciences, Beijing, China
[b] Key Laboratory of Meteorological Disaster of Ministry of Education, Nanjing University of Information Science and Technology, Nanjing, China
[c] Collaborative Innovation Center on Forecast and Evaluation of Meteorological Disasters, Nanjing University of Information Science and Technology, Nanjing, China
[d] National Satellite Meteorological Center, China Meteorological Administration, Beijing, China
[e] Tokyo University of Marine Science and Technology, Tokyo, Japan
[f] Atmosphere and Ocean Research Institute, The University of Tokyo, Kashiwa, Japan
[g] National Institute for Environmental Studies, Tsukuba, Japan
[h] Earth Observation Research Center, Japan Aerospace Exploration Agency, Tsukuba, Japan

ARTICLE INFO

Keywords:
Dust emission
Dust direct radiative effect
Dust daily variation
Meteorology nudging

ABSTRACT

In this study, we present simulations of the global dust cycle for present day conditions using a new dust-atmosphere model based on the Non-hydrostatic Icosahedral Atmospheric Model (NICAM) coupled with the Spectral Radiation Transport Model for Aerosol Species (SPRINTARS). We focus on evaluations of the dust simulation with respect to emissions, depositions, surface concentrations, aerosol optical depths (AODs), and the dust-aerosol direct radiative effects (DREs). The sensitivities of the dust simulation to the meteorological fields are also investigated through with and without meteorological nudging. NICAM without meteorology nudging tends to systemically overestimate the 10 m wind speeds by approximately 30%–40%, whereas the daily magnitudes and variations in the 10 m wind speeds are both significantly improved with meteorological nudging, especially over the Sahara Desert. The estimated annual global mean dust emission flux, dust AOD, and dust-aerosol shortwave DRE at the top of the atmosphere with meteorological nudging are 1463 $Tg\,yr^{-1}$, 0.033, and -1.3 Wm^{-2}, respectively. Due to the approximately 30%–40% overestimations of the 10 m wind speeds over the two major desert regions, the estimated annual global mean dust emission flux, AOD, and DRE without meteorological nudging are significantly greater than those with meteorological nudging. The overestimations of 10 m wind speeds and the associated dust emissions are mainly caused by the positive biases of wind speeds especially from surface to approximately 2 km and slightly affected by the temperature fields. The monthly variations in the dust depositions over the Atlantic and the surface dust concentrations over the Pacific are all better simulated with meteorological nudging. Compared to both the AERONET (Aerosol Robotics Network)- and MODIS (Moderate-Resolution Imaging Spectroradiometer)- retrieved AODs, the simulated daily AOD variations are significantly improved with meteorological nudging, especially over the dust-aerosol dominated regions. The global and annual mean dust lifetime and size distribution, which are two critical factors for estimating dust radiative effects, are quite similar between the dynamic and nudged NICAMs. We therefore can use the dynamic model to understand climate-dust interactions in a global and annual scale. Furthermore, we can improve the model performances for some applications in regional and seasonal scales by meteorological nudging which probably cannot be achieved by just tuning the dust emission.

1. Introduction

Dust aerosols play an important role in shaping the Earth's climatic system. Over 50% of the global production of tropospheric aerosol particles in mass is composed of mineral aerosols, which are mainly from deserts and their border regions (Andreae et al., 1986). Due to its scattering and absorption of solar shortwave and surface longwave radiation, mineral dust has a large impact on the global radiation budget

* Corresponding author. Institute of Atmospheric Physics, Chinese Academy of Sciences, Beijing 100029, PR China.
E-mail address: daitie@mail.iap.ac.cn (T. Dai).

https://doi.org/10.1016/j.atmosenv.2018.07.016
Received 27 November 2017; Received in revised form 5 July 2018; Accepted 9 July 2018
Available online 10 July 2018

(Sokolik et al., 2001; Tegen, 2003; Chen et al., 2017). Through direct and indirect forcing, mineral dust can change the global temperature at the surface and in the atmosphere, which then affects precipitation and, thus, the dust-aerosol cycle (Miller et al., 2003; Huang et al., 2006a, 2006b; Yoshioka et al., 2007; Yin and Chen, 2007; Han et al., 2009). Dust can also be involved in cloud development, serving as cloud condensation nuclei (CCN) and ice nuclei (IN) (Liu et al., 2012b; Twohy et al., 2009). The long-distance transport of dust also has a significant effect on the marine ecological environment due to its biogeochemical role. The deposition of dust provides the micronutrient iron to the ocean and, thus, fertilizes the phytoplankton and drives atmospheric CO_2 decreases (Ridgwell, 2002). Deposition of dust on snow surface can also affect the snow albedo and modify the surface water and energy cycles, known as snow darkening effect (Wu et al., 2018a). In addition, mineral dust is critical for the assessment of air quality through the concentration of particulate matter and its impact on visibility (Jiménez-Guerrero et al., 2008).

To understand the impacts of dust, the global spatiotemporal distributions of dust should be studied. Direct observational data provides a wide range of detailed information about the aerosol but are representative of limited spatial and temporal scales (Prospero, 1999). Satellite measurements complement ground-based observations by providing greater spatial coverage, but challenges are still associated with this dataset in terms of the uncertainties and difficulties in the data retrieval processes (Ginoux et al., 2012). Therefore, dust models have become a significant tool for filling in the observational gaps when characterizing dust-aerosol spatiotemporal coverages, providing an efficient way to understand the climatic impact of dust aerosols (Woodward, 2001; Yue et al., 2010). Many dust models have been developed to simulate the emission, transport and distribution of dust at the global scale (Joussaume, 1990; Yue et al., 2009; Colarco et al., 2010; Astitha et al., 2012; Liu et al., 2012a; Peng et al., 2012). Dust emissions have important regional and global consequences and occur as episodic naturally driven processes on small spatial and temporal scales. Generally, the uplift of dust particles is expressed as a function of the surface wind speed and wetness (Ginoux et al., 2001). Dust particles are then transported by winds over long distances. The relative amounts of smaller particles to larger particles increase with increasing distance from the source as the larger particles are removed more quickly due to their higher settling velocities. The distributions of smaller particles are more diffuse because of their longer airborne lifetimes (Tegen and Fung, 1994). Dust from North Africa is often transported to the Atlantic, reaching as far as South America, the Caribbean, and the southern United States (Prospero, 1999; Gyan et al., 2005). Australia and Asia are the main sources of dust deposition in the Pacific Ocean, where the dust acts as a nutrient source. However, the long-term transport of dust is difficult to simulate well because of the hypotheses concerning the size distributions. A broad intercomparison of 15 global dust-aerosol models in AeroCom Phase I indicates that there are still large differences among the global models when simulating the dust cycle (Huneeus et al., 2011). Large uncertainties in both meteorology and source parameterization can substantially affect the global dust simulations (Ackerley et al., 2012; Astitha et al., 2012; Luo et al., 2003; Timmreck and Schulz, 2004), and better representations of dust emission and transportation have been recognized by nudging a simulation with reanalyzed meteorological parameters (Albani et al., 2014; Smith et al., 2017; Wu et al., 2016).

In this paper, we present the simulated global dust cycle using an aerosol module called the Spectral Radiation Transport Model for Aerosol Species (SPRINTARS) coupled with a new flexible resolution weather and climate model called the Non-hydrostatic Icosahedral Atmospheric Model (NICAM) in both dynamic and nudged versions. The simulated dust surface concentrations and deposition fluxes are validated using a benchmark dataset provided by the AeroCom project for cross-model inspections for the future development of dust models. The simulated aerosol optical depths (AODs) are also evaluated using ground-based and satellite-based observations. Finally, the dust-aerosol direct radiative effects (DREs) are computed and compared with other model results.

We start by describing the dust model and experiment setting in section 2. In section 3, we display the simulated results including the dust emission fluxes, depositions, surface concentrations, the dust AODs, and the dust-aerosol DREs. The comparisons of the simulations and observations are also outlined, focusing on the depositions, surface concentrations and daily dust AODs. Section 4 summarizes our findings and concludes the study.

2. Model description and experiments

NICAM uses a non-hydrostatic dynamic core and an icosahedral grid configuration (Tomita and Satoh, 2004; Satoh et al., 2008, 2014), making it suitable to run with flexible horizontal resolutions of coarse (approximately 200 km) to high (approximately 1 km) values on a supercomputer. Higher resolution grids are recursively subdivided from a coarser resolution grid. NICAM can also be adapted to run partially high resolution simulations that target particular areas with the stretched icosahedral grid system (Tomita, 2008; Goto et al., 2015). NICAM has been shown to reproduce a realistic multiscale cloud structure from the meso-scale to a planetary-scale cloud organization that is associated with the Madden-Julian Oscillation (MJO) (Miura et al., 2007). NICAM was also the first model to produce a global simulation with a horizontal grid spacing of less than 1 km (Miyamoto et al., 2013). More detailed descriptions of NICAM were presented by Satoh et al. (2014). In this study, we perform the global simulation with a horizontal resolution of 223 km (a total of 10,242 grid points) and a vertical resolution of 40 layers from surface to approximately 40 km altitude. The vertical grid spaces in the troposphere of approximately 160 m near the surface, exponentially increasing to approximately 1320 m around 16 km. We consider the aerosol DREs based on the two-stream k-distribution radiation scheme implemented in NICAM, which incorporates scattering, absorption, and emissivity by aerosol and cloud particles as well as absorption by gaseous compounds (Nakajima et al., 2000; Sekiguchi and Nakajima, 2008). For cloud formation processes, we use a large-scale condensation scheme (Le Trent and Li, 1991) and the Arakawa-Schubert type cumulus convection scheme (Arakawa and Schubert, 1974; Pan and Randall, 1998). The aerosol effects on cloud microphysical properties are included and successfully simulated by NICAM (Sato et al., 2018; Suzuki et al., 2004). The vertical turbulent scheme used in this study comprises an improved Mellor-Yamada turbulence closure scheme (Mellor and Yamada, 1982; Nakanishi and Niino, 2006; Noda et al., 2010). The used land surface model named minimal advanced treatments of surface interaction and runoff (MATSIRO) (Takata et al., 2003) is online coupled with NICAM.

The SPRINTARS (Takemura et al., 2000, 2005, 2009), which was originally coupled to the Model for Interdisciplinary Research on Climate (MIROC), has been used in global aerosol model comparisons since the initial AeroCom assessment (Kinne et al., 2006; Textor et al., 2006). SPRINTARS treats evolutions of various species of aerosols in the atmosphere, including soil dust, organic carbon, black carbon, sulfate, and sea-salt aerosols, and it has been implemented in NICAM (Suzuki et al., 2008). In NICAM-SPRINTARS, bulk aerosol mass of sulfate and carbonaceous aerosols are predicted by considering the emission, transport, and deposition processes, whereas sea salt mass is tracked in 4 bins (Dai et al., 2014; Takemura et al., 2000). The emission inventories used in this study are from the AeroCom-II ACCMIP datasets (Lamarque et al., 2010) (http://aerocom.met.no/download/emissions/AEROCOM-II-ACCMIP/). Sea salt emissions are calculated online mainly depending on the near-surface wind speeds (Takemura et al., 2009). To calculate the sulfate chemistry (Takemura et al., 2000), the oxidants (ozone, hydroxyl radicals, and H_2O_2) are from an offline global chemical transport model (Sudo et al., 2002). In the aerosol coupled NICAM, dust aerosols are divided into 10 bins by particle radii, ranging

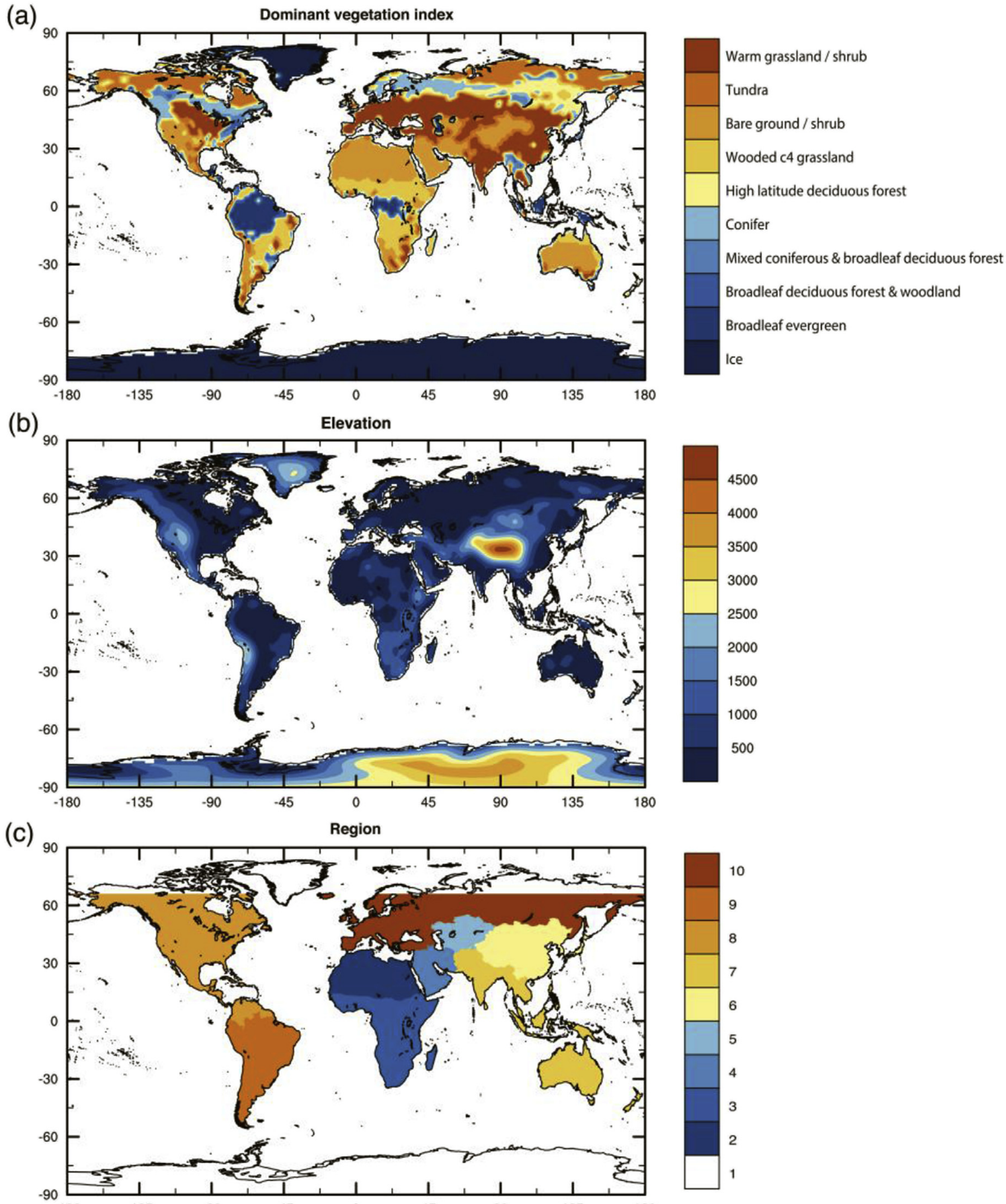

Fig. 1. Horizontal distributions of the static parameters associated with the dust simulation, including the (a) dominant vegetation index, (b) topography, and (c) defined regions used by NICAM.

from 0.1 to 10 μm (Takemura et al., 2000). The natural dusts of the bare ground areas (Fig. 1a) are emitted to the modeled planetary boundary layer with a constant mixing ratio, wherein all three of the following conditions are satisfied: (1) the wind speeds at the 10 m height (v_{10}) are over the threshold velocity, (2) the soil relative moisture (W_g) is dryer than the threshold moisture, and (3) the surface snow amount is less than 1 kg/m^2. The emitted dust mass fluxes (F) are calculated online at each model integration step (i.e., 20 min in this study) wherein the parameterization is set as the following empirical formulation (Takemura et al., 2009),

$$F = f(r)C_d\left(\frac{W_{gt} - W_g}{W_{gt}}\right)(|v_{10}| - u_t)\,|v_{10}|^2 \tag{1}$$

where $f(r)$ is the normalized emission strength of each size bin (Takemura et al., 2000); C_d as shown in Table 1 are empirically specified coefficients depending on ten regions to separate the main global deserts (Fig. 1c); u_t is the 10 m wind speed threshold velocity currently set to be 6.5 m/s for all bins, which is needed to be improved in future work because a size-independent threshold velocity is not fully supported by observations (Bagnold, 1941) and can bias the dust response to climate change (Hopcroft et al., 2015); W_{gt} is the threshold soil

Table 1
Empirically specified coefficients of dust emissions for the ten different regions, as shown in Fig. 1c.

Region	Coefficients of dust emission (C_d)
1	0.0
2	2.0×10^{-9}
3	8.0×10^{-10}
4	2.0×10^{-9}
5	2.0×10^{-9}
6	1.0×10^{-9}
7	8.0×10^{-10}
8	8.0×10^{-10}
9	8.0×10^{-10}
10	0.0

relative moisture set to be 0.1 except Asian desert region set to be 0.2. The higher W_{gt} over Asian desert is due to the soil moisture over this region is generally over than 0.1 (Figs. 2 and 3d). Here, the ν_{10} and W_g are both calculated with the online coupled land surface model MATSIRO. A three-dimensional icosahedral grid advection scheme preserving monotonicity and consistency with continuity for dust transport is adopted in NICAM (Niwa et al., 2011). The depositions of dust in NICAM are parameterized as same as in Takemura et al. (2000), including three processes: i.e., wet deposition, turbulent dry deposition, and gravitational settling (sedimentation). The wet deposition is further divided into two processes: i.e., the sub-cloud scavenging and in-cloud scavenging.

As same as the AeroCom Phase II for the present-day "control" experiments (http://aerocom.met.no/), we also mainly focus on the dust cycle for the year of 2006 in this study. Two versions of NICAM, i.e., with and without meteorological nudging, are used to investigate the sensitivity of the dust cycle to the NICAM-simulated meteorological fields. With the free-running version (DYNAMIC), NICAM coupled with a simple mixed layer ocean model predicts the meteorological fields with a new dynamic core of fully compressible and non-hydrostatic equations for five years since 2006 forced by the prescribed NCEP monthly mean sea surface temperature (SST) and sea ice fraction without any meteorological nudging, as were the studies of the aerosol interactions with clouds, meteorology, and climate, which is preferable to run the dynamic model freely or at least retain the characteristics of the free-running model (Zhang et al., 2014). In the nudged version (NDG_UVTQP), NICAM is run for one year in the same way as in the DYNAMIC except for the additions of wind (u, v), pressure (p), temperature (t), and specific humidity (q_v) nudging, which is implemented by the inclusion of the reanalysis data every 6 h from the NCEP Final (FNL) Analysis (NOAA/NCEP, 2000) (https://rda.ucar.edu/datasets/ds083.2/). Meteorological nudging is a simple assimilation technique that can facilitate a more straightforward comparison of simulations and observations and that can reduce the uncertainties associated with the discrepancy in large-scale circulations by constraining the climate model-simulated meteorological fields using reanalysis data (Zhang et al., 2014; Wu et al., 2018b). The implementation of nudging in NICAM uses the Newtonian relaxation method to constrain the dynamical state by adding a forcing to the prognostic equations that relaxes

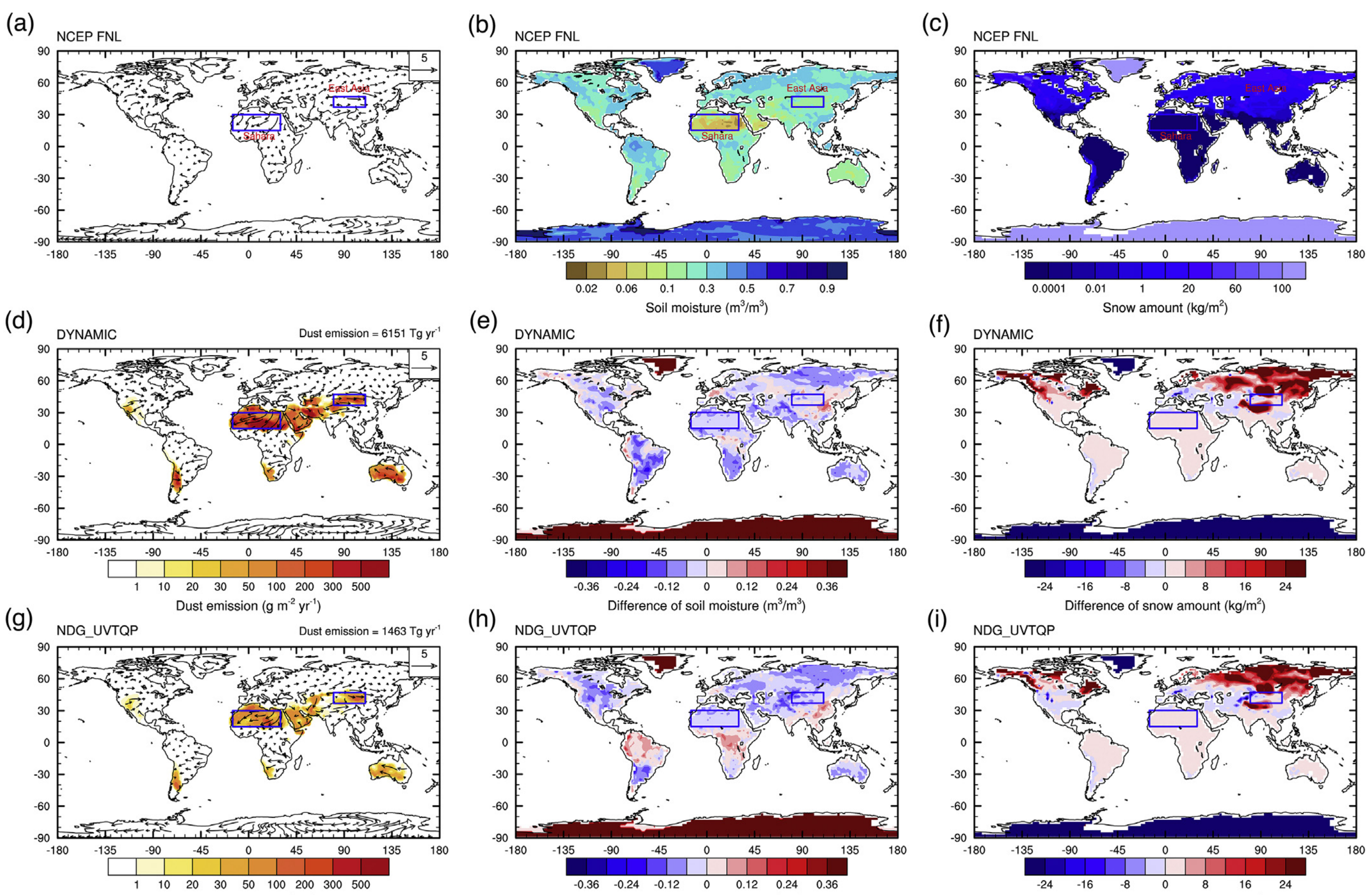

Fig. 2. Spatial distributions of the annual mean 10 m wind field (a), soil moisture (b), and snow amount (c) over land for the NCEP FNL reanalysis data. The spatial distributions of the NICAM-simulated annual mean dust emission and 10 m wind field over land for the DYNAMIC (d) and NDG_UVTQP (g) experiments. The annual mean differences of the NICAM-simulated soil moisture and snow amount minus the NCEP FNL reanalysis ones for the DYNAMIC (e, f) and NDG_UVTQP (h, i) experiments. Two major desert regions, i.e., the Saharan (15°N-30°N and 15°W-30°E) and East Asian (37°N-47°N and 80°E – 110°E) deserts, are defined as the rectangle areas.

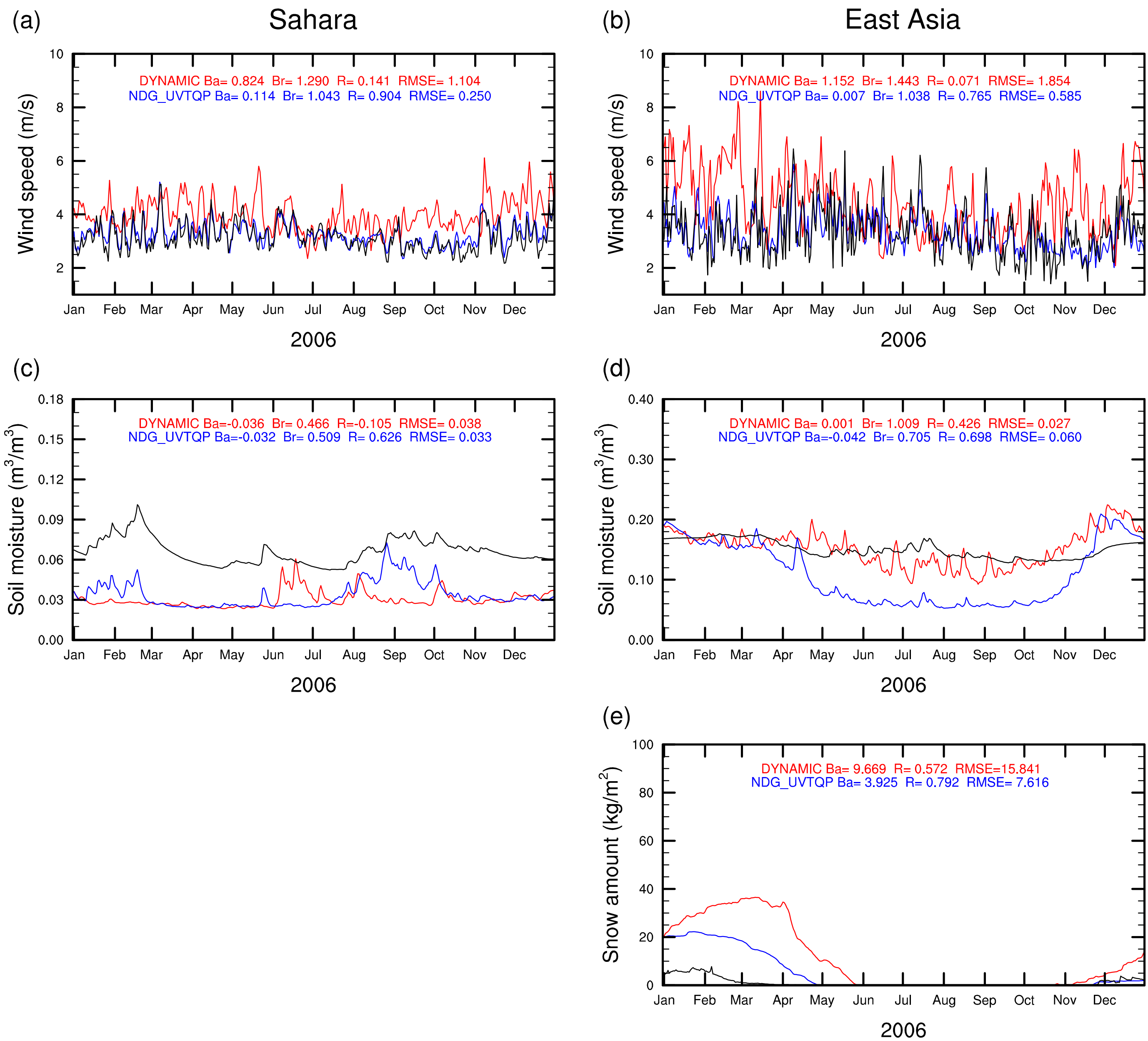

Fig. 3. Comparisons of the area and daily mean 10 m wind speed, soil moisture and snow amount from the DYNAMIC, NDG_UVTQP and the NCEP FNL reanalysis data in Saharan (a), (c) and East Asian desert (b), (d), (e). There is no snow in Saharan desert. The two major desert regions are defined as the rectangular areas in Fig. 2. B_a, B_r, R and RMSE represent the mean bias, relative difference, correlation coefficient and root mean square error, respectively.

the model toward prescribed atmospheric conditions (Stauffer and Seaman, 1990). The nudging coefficient τ for all variables above the model 10 levels is set to 0.000046 s corresponding to a timescale of 6 h (Zhang et al., 2014), and it smoothly decreases to zero from level 10 to level 1 as in equation (2) below,

$$\tau = \begin{cases} \frac{1}{2}\left(1.0 + \cos\left(\frac{z(10) - z(k)}{z(10) - z(1)}\pi\right)\right) \times 0.000046 & 1 \le k < 10 \\ 0.000046 & 10 \le k \le 40 \end{cases} \tag{2}$$

where z is the height of the model level. For the purpose of understanding dust-climate interactions and looking at past or future change, we need to use the dynamic model to simulate the meteorological fields, however, meteorological nudging ensures the simulations are closer to the real meteorology. Therefore, information about possible differences between the dynamic and nudged versions are important for our understanding of the meteorological parameters effects on global dust cycle simulations and the associated uncertainties on estimation of the climate effect of dust.

3. Results

3.1. Dust emission flux

Fig. 2 shows the comparisons between the NICAM simulated and NCEP FNL reanalysis annual mean 10 m wind fields, soil moisture, and surface snow amount for the year 2006 by the two NICAM versions. The spatial distributions of the simulated annual mean dust emission fluxes are also shown in Fig. 2. Compared to the NCEP FNL reanalysis fields, we find that both the two versions of model can generally reproduce the main horizontal structures and magnitudes of the annual mean 10 m wind fields, soil moisture, and surface snow amount especially over the Saharan and East Asian desert regions, indicating that NICAM can simulate the climatic characteristics of land surface and atmospheric parameters for dust emission estimations. However, there are considerable discrepancies between the two versions of the estimated dust emission fluxes, which have annual global mean values of 6151 Tg yr^{-1} and 1463 Tg yr^{-1}. The interannual variability of the global mean dust emission fluxes calculated by the standard deviation of dust emission during the 5-year simulation relative to the mean of 5-year simulation is 3.8% using the dynamic version, indicating the large discrepancy of the dust emissions between the dynamic and nudged versions are not mainly caused by the interannual variability of the dust emissions. The major dust source areas are clearly located over the Sahara Desert, the Arabian Peninsula and the Gobi Desert. Since the dust emission strengths are mainly dependent on the 10 m wind speeds (Mukai et al., 2004) and there are few observational data points available for validation, the simulated daily area average 10 m wind speeds over the two major dust source regions, i.e., the Saharan and East Asian desert regions as defined by the rectangular areas in Fig. 2, are compared with the NCEP FNL data, as shown in Fig. 3. It is also proved that the soil moisture and snow cover can affect the dust emission predictions over Asian desert especially over the snow-melting season (Tanaka et al., 2011; Wu et al., 2016), therefore, the NICAM simulated soil moisture and snow amount are also shown in Fig. 3. The nudged NICAM (NDG_UVTQP) significantly improves the simulated 10 m wind speeds. The correlation coefficients (R) between the NICAM-simulated and the NCEP FNL daily 10 m wind speeds over the Saharan and the East Asian desert regions increase from 0.141 and 0.071 to 0.904 and 0.765, respectively. The mean biases (B_a), relative differences (B_r), and root mean square errors (RMSE) between the simulated and NCEP FNL reanalysis daily 10 m wind speeds over both regions are also improved. Over the Saharan desert region, the dynamic NICAM (DYNAMIC) tends to overestimate the 10 m wind speeds, with B_a and B_r values of 0.824 and 1.290, respectively, whereas the nudged NICAM correctly reproduces the reanalysis 10 m wind speeds, with B_a and B_r values of 0.114 and 1.043, respectively. Over the East Asian desert region, the DYNAMIC also tends to overestimate the 10 m wind speeds, with B_a and B_r values of 1.152 and 1.443, respectively, and the NDG_UVTQP reduces the B_a and B_r to values of 0.007 and 1.038, respectively. Reproducing the 10 m wind speeds over the East Asian desert region, even with nudging technique, is even more difficult, which is likely caused by the more complex topography over the Eastern Asian desert region, as shown in Fig. 1b. Due to the limitation of describing the topographic characteristics with a coarse resolution model, the model is unable to capture all the wind variability caused by the complex topography in the Eastern Asian desert region, which reflects in the higher RMSE and lower R compared to the Saharan desert region. With respect to the soil moisture, it is found that both versions of NICAM can reproduce dryer soil moisture over the Saharan desert than that over the East Asian desert. Over the Saharan desert, both versions of NICAM tend to underestimate the soil moisture with similar magnitude. Over the East Asia desert, the nudged NICAM tends to produce dryer soil moisture especially in summer months. The meteorological nudging can also improve the capability of NICAM to simulate the temporal variations of soil moisture as indicated by the higher R over both the Saharan and East Asian Deserts. There is no snow cover over the Saharan desert in both NICAM and NCEP FNL data, and NICAM can generally reproduce monthly variation of the snow amount over Eastern Asia desert although both versions of NICAM tend to overestimate the snow amount. It is found that there are significantly positive biases of wind speeds especially from surface to approximately 2 km with the dynamic NICAM over both the Saharan and East Asian desert regions (figure not shown for brevity), indicating the overestimation of the 10 m wind speed is probably caused by the overestimation of wind speed in dynamic NICAM. We perform other four experiments with different nudging strategies (Table 2) to further investigate the possible effects of wind, temperature, humidity, and pressure on the overestimations of the 10 m wind speeds over the two major desert regions. The estimated annual global mean dust emission flux of 1463 Tg yr^{-1} in the NDG_UVTQP is generally consistent with the

Table 2
Experimental design for the sensitivity test in this study.

Sensitivity experiments
DYNAMIC: NICAM is freely run for 5 years since 2006 forced by the NCEP monthly mean sea surface temperature (SST) and sea ice fraction, and not nudging any meteorological fields
DYNAMIC_TUNING: Same as DYNAMIC except reducing the empirically specified coefficients C_d over all regions by a factor of 4.2
NDG_UV: NICAM is run for 1 year since 2006 forced by the NCEP monthly mean SST and sea ice fraction, and wind (u, v) are nudged to match the NCEP FNL reanalysis data every 6 h
NDG_UVT: Same as NDG_UV but wind (u, v) and temperature (t) are nudged
NDG_UVTQ: Same as NDG_UV but wind (u, v), temperature (t) and specific humidity (q_v) are nudged
NDG_UVTQP: Same as NDG_UV but wind (u, v), temperature (t), specific humidity (q_v) and pressure (p) are nudged

value of 1383 Tg yr^{-1} derived by assimilating the observed aerosol optical depth in a global aerosol model (Huneeus et al., 2012) and the mean of the AeroCom models (Table 3) (Textor et al., 2006; Colarco et al., 2010). Both the better simulations of the 10 m wind speeds and global dust emission flux of NDG_UVTQP indicate the coefficient C_d (Table 1) used in NICAM are reasonable. The distribution characteristics of the other dust sources in the south of Africa, northern America, South America, and Australia are also found to be similar to those of other global dust models (Chin et al., 2009; Yue et al., 2009). To mitigate the overestimation of dust emission with the dynamic NICAM, one more experiment named as DYNAMIC_TUNING is performed in the same way as in the DYNAMIC except for reducing the C_d over all regions by a factor of 4.2. The reduced factor of 4.2 is calculated as the ratio of annual global mean dust emissions between the DYNAMIC and NDG_UVTQP. As shown in Fig. 4, the experiment with only nudging the winds can effectively reduce the overestimations of the 10 m winds and dust emissions over both the two desert regions. The experiment with nudging both the winds and temperature further slightly reduces the overestimations and generally produces the similar results as the experiments of NDG_UVTQ and NDG_UVTQP. We therefore conclude that the overestimations of 10 m winds and the associated dust emissions are mainly caused by the positive biases of wind speeds and slightly affected by the temperatures. As shown in Table 4, the dust emissions have the highest relationships with the 10 m wind speeds compared to the soil moisture and snow amount over both the Saharan and East Asian deserts, further indicating the 10 m wind speed is the most important factor for dust emission. The dust emissions over East Asian desert are also affected by the snow amount, such as there are slightly differences of dust emissions over the winter months (due to snow covers suppress the dust emissions) even when the wind speeds have significantly differences. The occasionally significant differences of the wind speeds between the two dynamic experiments especially over the East Asian desert in spring months indicate the suspended dusts may significantly modify the atmospheric fields through dust direct and/or indirect effects and consequently change the dust emission fluxes (i.e., the dust emission flux in DYNAMIC_TUNING may be different with that in NDG_UVTQP). As shown in Fig. 5, the correlations between the simulated 6 hourly instantaneous meteorological patterns over all model grids with those interpolated from the NCEP FNL reanalysis are compared. Generally speaking, NICAM dynamical core has the best capability to reproduce the NCEP FNL temperatures and it has more difficulty in reproducing the wind field. The nudging of the winds can not only significantly improve the wind fields but also the temperature fields, and the nudging of additional temperatures can slightly improve the simulation of wind fields. The nudging strategy with including the specific humidity can best reproduce the “real” specific humidity fields. Therefore, the experiment of NDG_UVTQP generally represents the simulation that is mostly close to the real meteorology for dust emission, transport, and deposition. Hereafter, we show only detailed results for

Table 3
Simulated mass balance of dust aerosols.[a]

Experiment	Emission [Tg yr^{-1}]	Burden [Tg]	Deposition [Tg yr^{-1}]	Wet Depo [Tg yr^{-1}]	Dry Depo [Tg yr^{-1}]	Life Time [days]
DYNAMIC	5813	62.9	5830	2273	3557	3.94
DYNAMIC_TUNING	1670	20.0	1685	769	916	4.33
NDG_UVTQP	1463	18.4	1522	781	741	4.41
AeroCom Mean	1789	19.2	1950	626	1324	4.22
AeroCom Range	541–4036	1.4–33.9	676–4359	295–1382	302–3356	0.92–18.4

[a] Note. Wet Depo represents the wet deposition. Dry Depo represents the dry deposition including both the turbulent dry deposition and sedimentation.

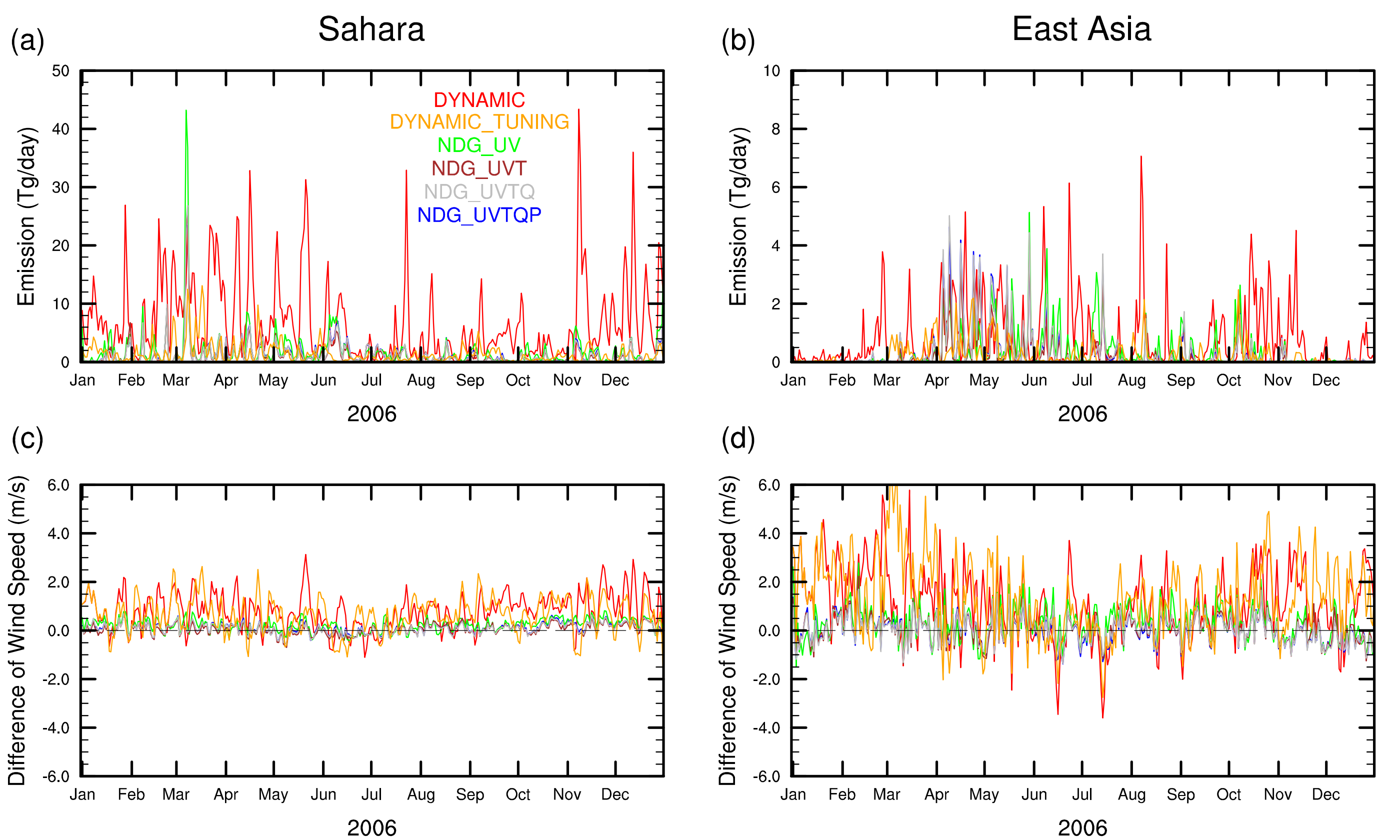

Fig. 4. The NICAM-simulated area and daily mean dust emissions in Saharan (a) and East Asian desert (b). The daily average differences of the NICAM-simulated 10 m wind speeds minus the NCEP FNL reanalysis ones averaged over the two major desert regions are also given in (c) and (d), respectively. Both the simulated and reanalysis daily mean values are simply averaged by the 6 hourly instantaneous values.

Table 4
Correlation coefficients between the dust emissions and the meteorological parameters in the selected source regions.[a]

Source region	10 m wind speed	soil moisture	snow amount
Sahara	0.749 ± 0.067	−0.167 ± 0.016	NaN
East Asia	0.536 ± 0.077	−0.094 ± 0.065	−0.092 ± 0.079

[a] Note. The values represent the mean correlation coefficient and standard deviation calculated by all the six experiments in Table 2.

the experiments of DYNAMIC, DYNAMIC_TUNING, and NDG_UVTQP for simplicity.

3.2. Dust lifetime and depositions

The dust lifetime generally reflects the dust cycle and significantly depends on sink processes (i.e., dry and wet depositions). Therefore, the evaluation of the dust lifetime helps to explain the differences in the simulated dust fields that are caused by aerosol processes rather than by emission strengths (Textor et al., 2006). The dust lifetime is computed as the dust burden (i.e., the column integrated dust mass concentrations) divided by the loss rate sink (Textor et al., 2006; Colarco et al., 2010).

Table 3 summarizes the NICAM-simulated annual global mean dust emissions, burdens, depositions, and lifetimes of the three experiments, and the associated AeroCom means and ranges are also given for comparison (Colarco et al., 2010; Huneeus et al., 2011). Notably, the corresponding mean results over the five years of the dynamic experiments except the AOD for the specific year 2006 are used for comparisons hereafter. The dust emissions, burdens, and depositions of NDG_UVTQP and DYNAMIC_TUNING are all comparable to those of the AeroCom mean, indicating that NICAM-simulated dust cycle is generally reasonable with both the dynamic and nudged versions. Keeping in mind that the dust emissions are overestimated in DYNAMIC due to its overestimations of the 10 m wind speeds, it is not surprising that the dust burden and dry and wet depositions are even larger than those in the upper range of AeroCom. The dry deposition is less than the wet one in nudged version, whereas the dry deposition is larger than the wet one in dynamic version, indicating that the meteorological nudging

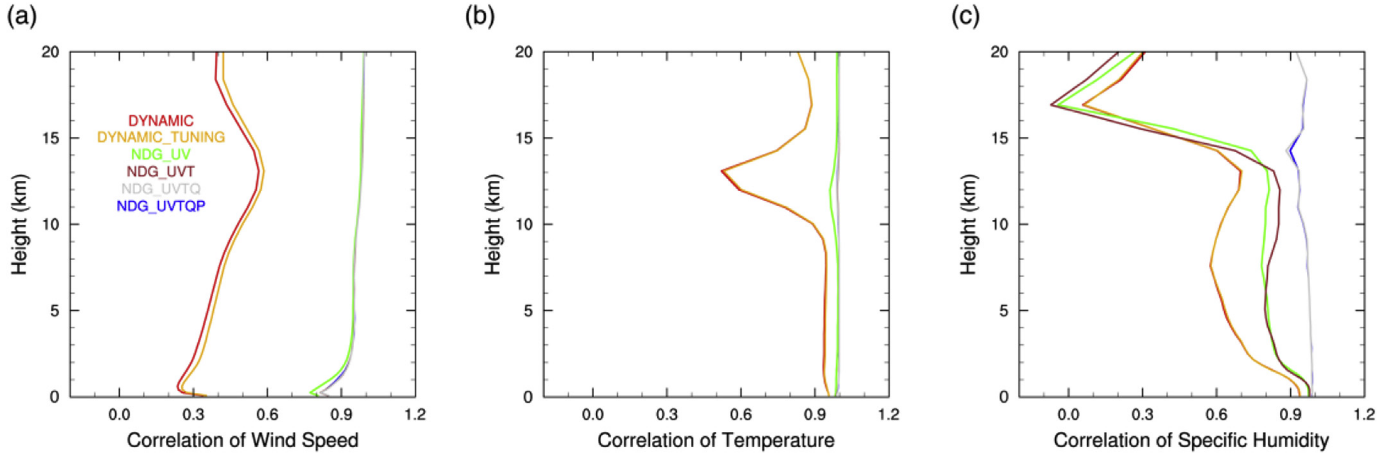

Fig. 5. The correlations of wind speed (a), temperature (b) and specific humidity (c) between the simulated 6 hourly instantaneous meteorological patterns over all model grids with those interpolated from the NCEP FNL reanalysis below 20 km.

technique probably enhances the relative contribution of the wet deposition of dust in NICAM, which is associated with the simulations of the cloud and precipitation processes. Detailed verifications of the modeled cloud and precipitation processes associated with the wet deposition of dust are beyond the scope of this study. Although the global dust emissions from the two dynamic experiments vary by more than a factor of three, the diversity of the dust lifetimes is smaller than half a day. The difference of dust lifetime between the DYNAMIC_TUNING and NDG_UVTQP is 0.08 days, which is even smaller than the difference between the two dynamic experiments. The ratio of the dry deposition to total deposition increases with dust emission over the two dynamic experiments, and this is probably due to the emissions of coarse dust particles predominant the total emissions and larger dust particles are removed more efficiently by dry depositions nearer the source regions. Because wet deposition shows longer lifetime compared to dry deposition, more efficient dry deposition can shorten the dust lifetime.

Dust deposition across the globe is a powerful constraint of the overall dust budget, yet direct observations of dust deposition remain scarce. Four freely available compilations of dust deposition fluxes (Huneeus et al., 2011), which represent to first order a modern or present-day climatology of dust deposition observations, are used to evaluate the simulated dust depositions. Although the interannual variability of dust in the main dust-source areas or outflow regions is generally small (Smith et al., 2017), it may induce discrepancy to compare simulation for a specific year with the climatology of observations. The first dataset is the dust deposition fluxes given in Ginoux et al. (2001), which are based partly on measurements taken during the SEAREX campaign in 1979 (Prospero et al., 1989). Most of the observation sites are located in the Northern Pacific Ocean, indicating the deposition of long-distance dust transports. The second dataset is from Mahowald et al. (2009) and is a compilation with a total of 28 sites that measure dust deposition. The third dataset is the depositional fluxes derived from the ice core data recorded in Greenland and Antarctica (Mahowald et al., 1999). The ice cores provide the best estimates of long-distance dust transports (Kohfeld and Harrison, 2001). The last dataset ThoroMap is the deposition fluxes over global ocean recently built using thorium isotopes (Kienast et al., 2016). Comparisons of the measured and simulated total annual dust deposition fluxes are shown in Fig. 6. The locations of each data point in the scatter plot are given in Fig. 6a–d. The sites are marked in different colors and forms to represent their regions and data sources. The statistical criteria, such as R, B_a, RMSE, the ratio of the modeled and observed standard deviation (sigma), normalized root mean square error (NRMS), and mean normalized bias (MNB), are also calculated to quantify the model performance (Boylan and Russell, 2006; Huneeus et al., 2011). The NRMS and MNB are calculated as follows:

$$NRMS = \sqrt{\frac{1}{N}\sum_{i=1}^{N}\left(\frac{m_i - o_i}{o_i}\right)^2} \tag{3}$$

$$MNB = \frac{1}{N}\sum_{i=1}^{N}\frac{m_i - o_i}{o_i} \tag{4}$$

where N is the number of stations considered, m_i and o_i are the simulated and observed values at station i respectively. The biases of most stations are within a factor 10 of the observations in all the three experiments, and the dust depositions are generally better simulated in DYNAMIC_TUNING than that in DYNAMIC, especially over the Sahara Desert outflow regions. In DYNAMIC, the depositions over most stations near the west coast of Northern Africa are more than a factor of 10 greater than those observed, indicating overestimations of the Saharan dust emissions. The deposition fluxes over the Antarctic regions are overestimated in all the three experiments, a feature which is also commonly found in other global dust models (Huneeus et al., 2011). The depositions over the northern Pacific are generally comparable to the observations in all the three experiments, whereas the depositions over the tropic Pacific are significantly underestimated in NDG_UVTQP, indicating the underestimations are caused by the more efficient wet depositions near dust source areas in NDG_UVTQP.

To show the performance of the NICAM-simulated long-range dust transport across the Atlantic, the simulated wet and total dust depositions are further evaluated with observations from three stations of the Florida Atmospheric Mercury Study (FAMS) network (Prospero et al., 2010), as shown in Fig. 7. The three stations have similar longitudes. From south to north, the stations are LittleCrawlKey (24.75 N, 80.98 W), TamiamiTrail (25.77 N, 80.82 W) and LakeBarco (29.67 N, 82.02 W). Due to the effects of the prevailing westerly and subtropical high on the Saharan dust transport path, the wet and total dust depositions reach their peaks over the summer months (Ridley et al., 2012). Compared to the dynamic version (even tuning the dust emissions), the monthly variations in both the wet and total dust depositions over the three sites are clearly improved with the nudged version (NDG_UVTQP). One reason for this improvement may be due to the better simulations of the meteorological fields with the nudging technique and consequent better dust transport path (Fig. 5). Another explanation for this improvement may be due to the better simulation of the monthly variation of the dust source over the Saharan desert. It is obvious that the monthly variation of dust deposition over the summer months is linked to that of the dust emission over the Saharan desert (e.g., the significant overestimations of 10 m wind speeds in September of the DYNAMIC experiment correspond to the significant

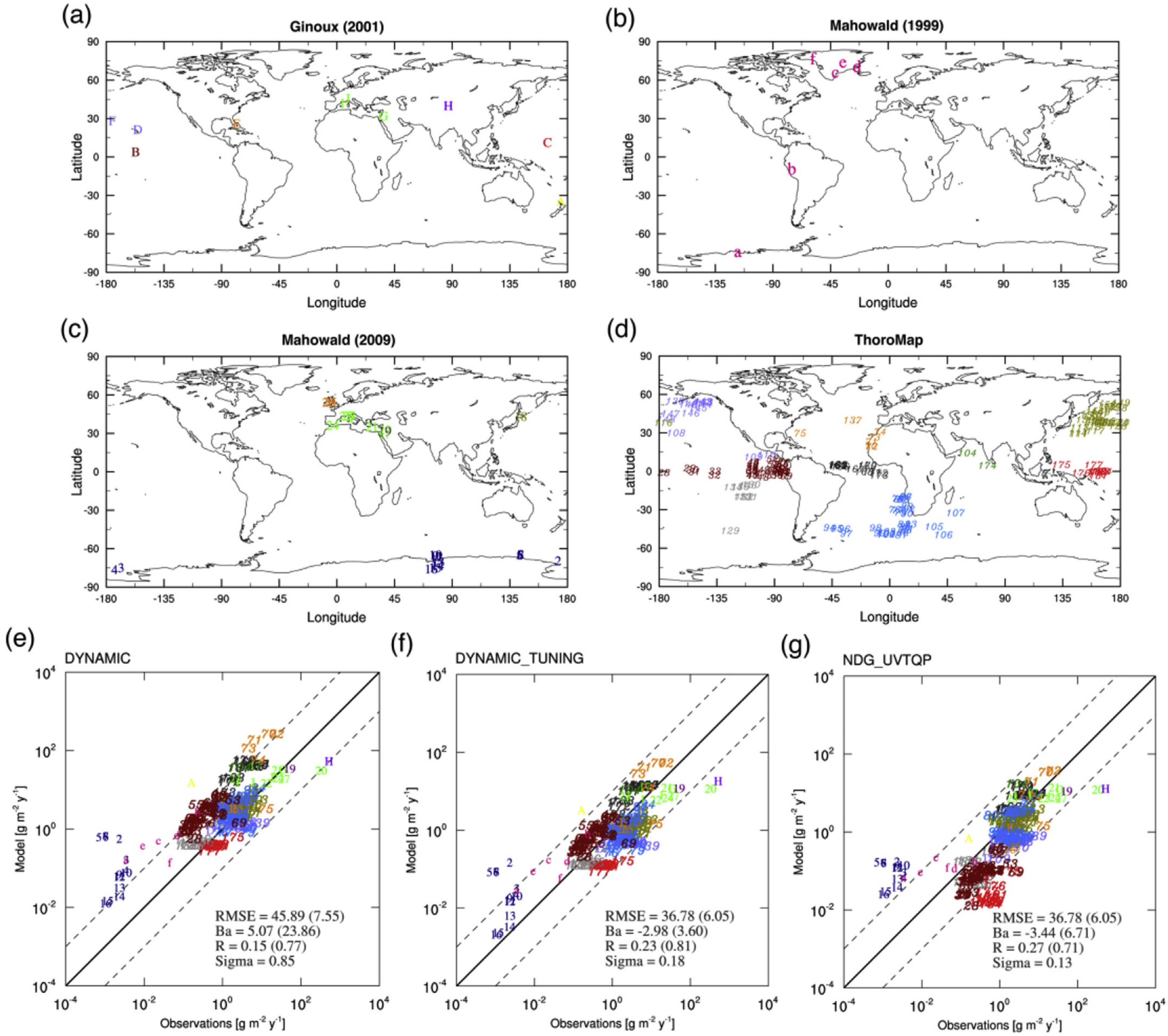

Fig. 6. The locations of each data point in the scatter plot from Ginoux et al. (2001)/Mahowald et al. (1999)/Mahowald et al. (2009)/ThoroMap are marked in (a), (b), (c) and (d). The four datasets are indicated with letters/lower-case letters/non-italic numbers/italic numbers, respectively. The numbers and letters are colored by region, including the North/Tropical/South Western Pacific (olive green/red/yellow), North/Tropical/South Eastern Pacific (violet/brown/grey), North/Tropical/South Atlantic (orange/black/light-blue), Asia/Europe (purple/light green), Indian/Southern Ocean (dark green/dark blue) and pink ice core data from Greenland, South America and Antarctica. Comparisons of the measured and modeled yearly depositional fluxes for DYNAMIC (e), DYNAMIC_TUNING (f) and NDG_UVTQP (g). Root mean square error (RMSE), mean bias (B_a), ratio of the modeled and observed standard deviation (sigma) and correlation coefficient (R) are shown in the lower right part of the scatterplot. The mean normalized bias and normalized root mean square error are given in the parenthesis next to RMSE and B_a, respectively. The correlation with respect to the logarithmic result of the model and of the observations is also given in parenthesis next to R. The black continuous line is the 1:1 line, whereas the black dotted lines correspond to the 10:1 and 1:10 lines. (For interpretation of the references to color in this figure legend, the reader is referred to the Web version of this article.)

overestimation of the deposition in September). The consistency of simulated and observed depositions deteriorates from south to north reflects the difficulties in northward transport simulations, which is also commonly found in other models (Huneeus et al., 2011).

3.3. Surface dust concentration

Surface dust concentration is an alternative metric for evaluating the performance of dust transports from source regions. As shown in Fig. 8, three stations that measured the surface dust concentrations over the East Asian dust transport path from the SEAREX exchange program (Prospero et al., 1989; Huneeus et al., 2011) are selected to evaluate the performances of the simulated monthly Asian dust variations. It is obvious that the nudged NICAM can better reproduce the magnitudes and monthly variations of the observations than the free-running ones over all the three stations. Over both the Hedo (26.92 N, 128.25 E) and Cheju (33.52 N, 126.48 E) stations, the DYNAMIC experiment tends to overestimate the surface concentrations in November due to the significant overestimations of the 10 m winds and consequent dust emissions over the East Asian desert regions (Figs. 3 and 4), which induce unreal bimodal distribution with one peak in April as the observation but unreal peak in November. Although the DYNAMIC_TUNING experiment

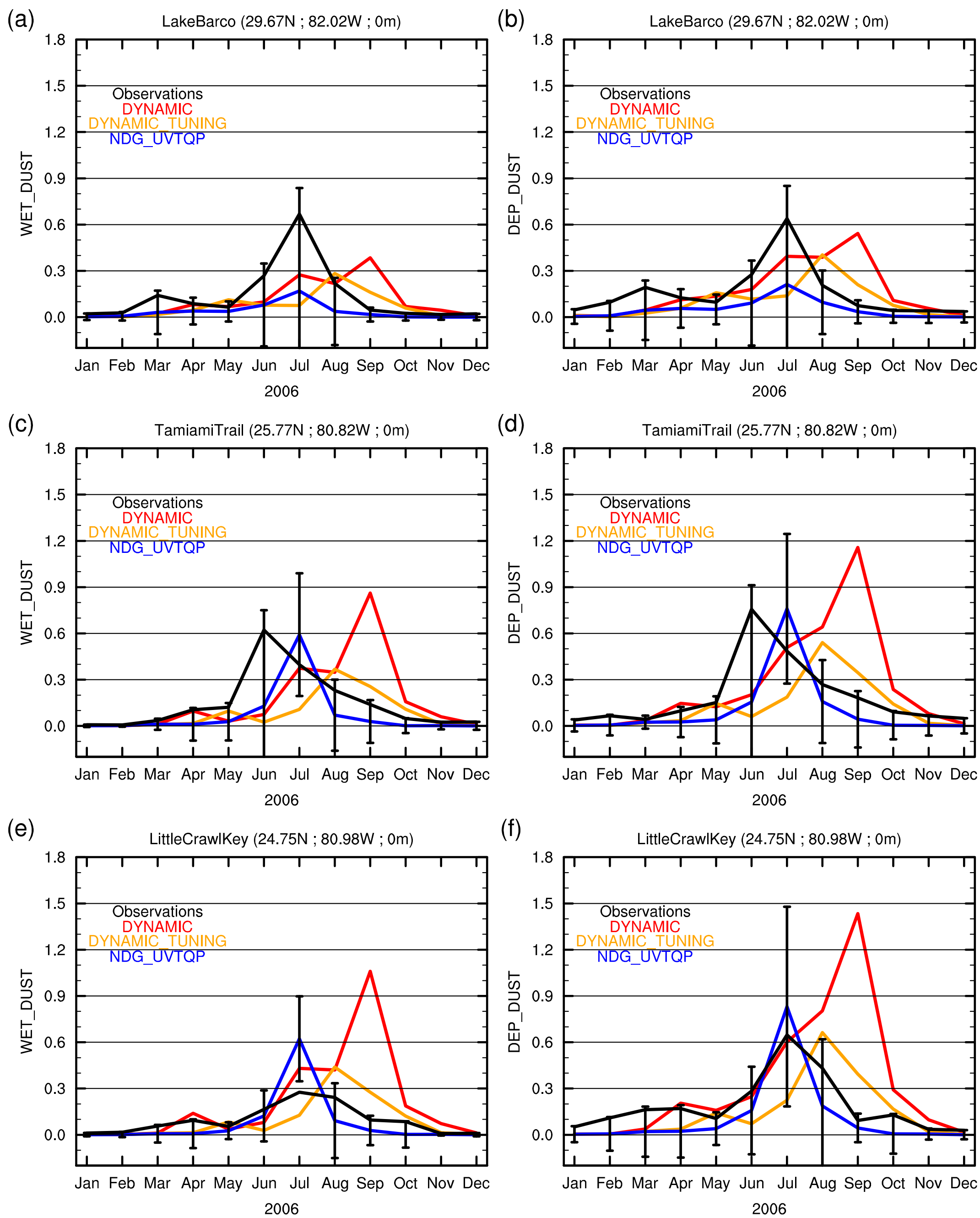

Fig. 7. Comparisons of the modeled and observed monthly accumulated wet (left column) and total (right column) dust deposition rates at the three stations from the FAMS network: LakeBarco, TamiamiTrail, and LittleCrawlKey. The units are g m^{-2} $month^{-1}$. The black line is the mean deposition rate during 1994–1996 from the FAMS network. The vertical lines represent the standard deviations.

corrects the unreal peak of surface dust concentrations in November, the simulated surface dust concentrations over the spring months are also significantly underestimated. Over the Midway Island (28.22 N, 177.35 E) station, the simulated surface dust concentrations in DYNAMIC experiment are generally higher than the observed ones in the whole year except February and November, even falling outside of the error bars of the observations, whereas the DYNAMIC_TUNING experiment correctly reduces the overestimations and generally falls in the ranges of observation uncertainties except over the summer months. The simulated magnitudes and monthly variations in the surface dust concentrations in nudged NICAM both agree well with the observed values.

3.4. Aerosol optical depth

Global AODs are routinely observed with both ground-based AERONET (Holben et al., 1998) stations and satellite-based MODIS platforms (Remer et al., 2005). The retrieved AODs provide valuable data for global aerosol model validations. The model-simulated dust AODs are significantly relied on the assumed microphysical characteristics of dust, such as the size distributions and the spectral refractive index. The dust AODs of NICAM in this study are derived from the modeled mass concentrations with the method as same as Dai et al. (2014). The simulated annual global mean dust AODs as well as the mass extinction efficiencies of the three experiments are compared with the AeroCom mean and ranges (Colarco et al., 2010), as shown in Table 5. The mass extinction efficiency is defined as the AOD divided by

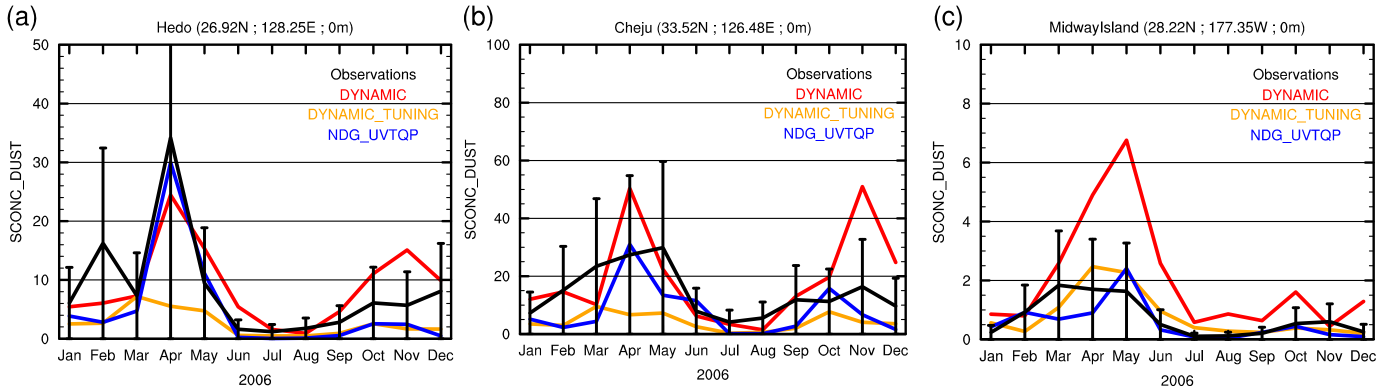

Fig. 8. Comparisons of the modeled and observed monthly mean surface dust concentrations at the (a) Hedo, (b) Cheju and (c) Midway Island stations; the units are $\mu g\ m^{-3}$.

Table 5
Annual global mean dust-AOD and mass extinction efficiencies.

Experiment	DUST AOD	Dust mass extinction efficiency (m^2g^{-1})
DYNAMIC	0.111	1.194
DYNAMIC_TUNING	0.035	1.198
NDG_UVTQP	0.033	1.295
AeroCom Mean	0.032	0.99
AeroCom Range	0.012–0.054	0.46–2.05

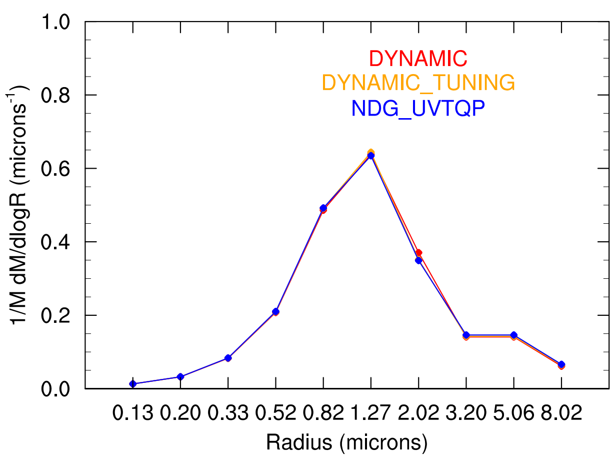

Fig. 9. Normalized annual and global mean column dust mass size distributions as a function of particle radius.

the column integrated dust mass concentration. Since dusts are assumed as hydrophobic aerosols, the dust mass extinction efficiency depends on the relative contribution of the dust concentration from each bin. The normalized annual and global mean column dust mass size distributions as a function of particle radius for the three experiments are shown in Fig. 9. The dust size distributions are quite similar between the dynamic and nudged NICAMs. The mass extinction efficiencies are comparable to the AeroCom mean and are within the AeroCom range, indicating that the dust optical parameters used in NICAM are reasonable. The annual global mean dust AODs of the DYNAMIC_TUNING and NDG_UVTQP are generally comparable to the AeroCom mean and are within the AeroCom range, whereas that of the DYNAMIC is 3.4 times higher than that of NDG_UVTQP and is over the upper range of the AeroCom models. The latter further proves that the dust emissions are overestimated in DYNAMIC.

As shown in Fig. 10, we select a total of 2427 daily mean AODs over 31 AERONET "dusty" stations, which are considered to be dominated by dust aerosols, to evaluate the simulated daily variations in dust AODs. The criteria for selecting the AERONET AODs in this study are defined as requiring at least 20 days at a specific AERONET station where both the daily mean AOD of 550 nm is greater than 0.2 and the daily mean Ångström Exponent is smaller than 0.4 in the year 2006. We use the logarithmic interpolation method to convert the 440 nm and 675 nm AODs of AERONET into 550 nm AODs to agree with the modeled AOD. The daily dust AODs are clearly overestimated in DYNAMIC, with B_a and RMSE values of 1.20 and 2.06, respectively. Compared with DYNAMIC, it is obvious that experiment NDG_UVTQP, with its nudging of the meteorological fields, significantly improved the ability of NICAM to simulate the daily dust variations, increasing the R from 0.15 to 0.50 and the simulated daily dust AODs to within a factor of two of the observations, improving from 34.9% to 72.5%. Compared to DYNAMIC, although the experiment DYNAMIC_TUNING can effectively reduce the significant overestimation of the daily mean AOD, however, it has a very limited effect on the simulation of daily dust variation as indicated by the similar correlation coefficients. Unlike the simulated daily mean AODs, the AERONET ones never observe the full diurnal cycle, therefore the representativeness of observations may affect the results of comparison (Schutgens et al., 2017). To consider the diurnal effect, we investigate the differences of the daily mean AODs averaged all times and other four ones averaged every 6-h from 0, 6, 12, and 18 UTC (Colarco et al., 2010). The differences between the daily mean AODs and the each 6-h AODs calculated by all the three experiments are mostly within ± 20% (the frequencies are higher than 78%), whereas the frequencies of differences between the simulated and observed ones within ± 20% are less than 30%. These results imply the diurnal variation in AOD does not affect our comparison significantly.

The Collection 6 (C6) MODIS-Terra Level 3 (L3) deep blue/dark target merged daily AODs (Levy et al., 2013; Sayer et al., 2013) are also used for evaluations. Fig. 11 show the spatial distributions of annual mean total AODs (i.e., sum of the dust AODs and all other non-mineral dust AODs) simulated by model and retrieved from the MODIS Terra. The effects of meteorological nudging on non-dust aerosol simulations are beyond the scope of this study. Compared to the MODIS AOD observations, the DYNAMIC_TUNING and NDG_UVQTP both reproduce more reasonable magnitudes and gradients than the DYNMAIC over the dust dominated regions such as the Saharan desert and the surrounding areas. In addition, the spatial distribution of annual mean AODs in NDG_UVTQP is more consistent with the MODIS-retrieved one than that in DYNAMIC TUNING. It is acknowledged that merely tuning the dust emission factors is not enough to reach the improvements in annual mean AODs as nudging the meteorological fields. Therefore, the implementation of the meteorological nudging technique not only lies in dust emissions but also lies in dust transport. The horizontal distributions of the correlation coefficients between the simulated daily mean total AODs and the MODIS-retrieved ones are also shown in Fig. 11. The slight differences between the DYNAMIC and DYNAMIC_TUNING demonstrate that simply tuning the dust emission factors can't improve

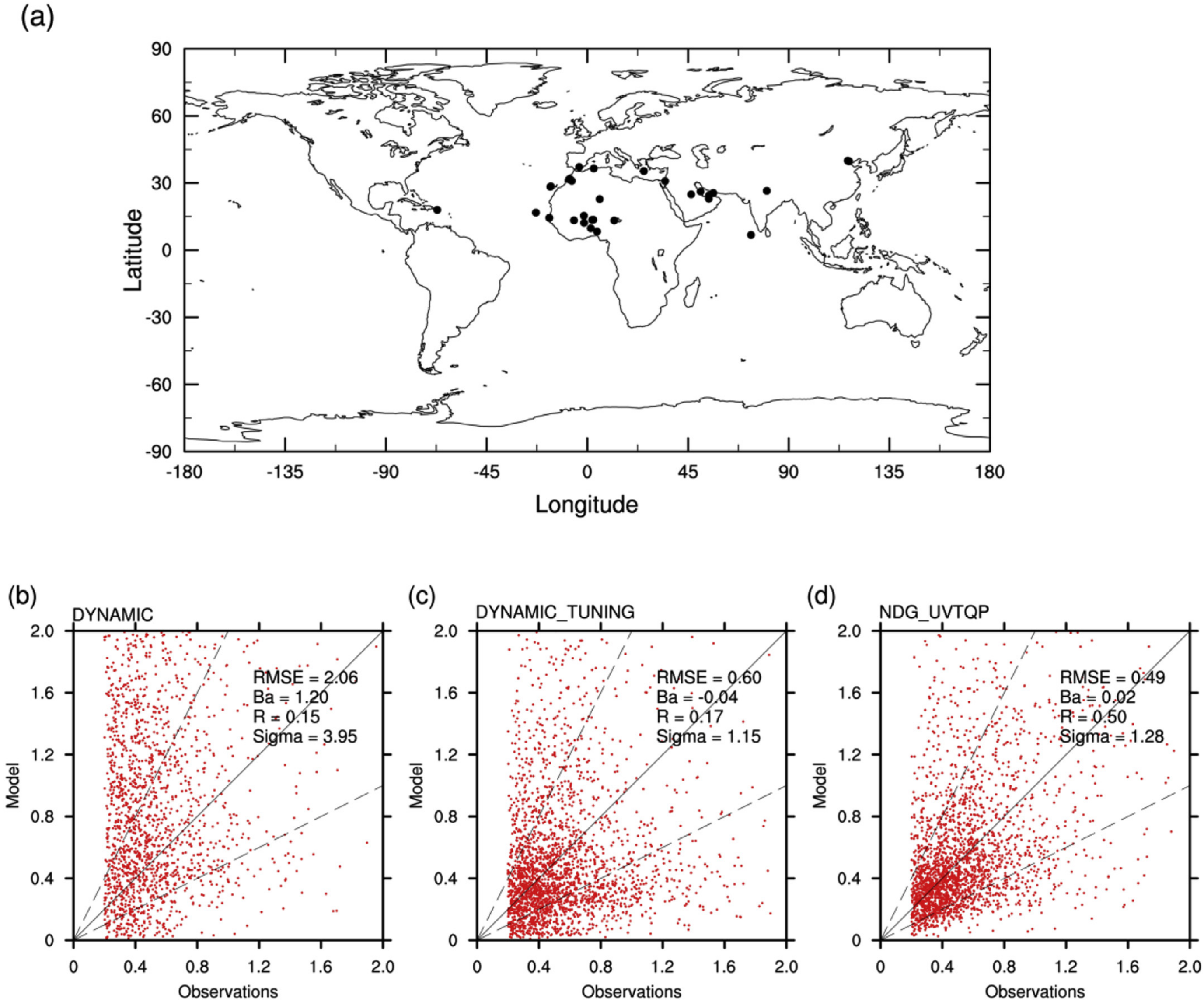

Fig. 10. (a) The locations of the "dusty" stations selected for comparison are marked. Comparisons of the modeled daily AODs and the AERONET ones over the "dusty" stations in 2006 for DYNAMIC (b), DYNAMIC_TUNING (c), and NDG_UVTQP (d). The black continuous line is the 1:1 line, whereas the black dotted lines correspond to the 2:1 and 1:2 lines.

the model capability of simulating aerosol temporal variations. With the implementation of the meteorological nudging technique, the correlations between the simulated daily total AODs and the MODIS-retrieved ones raise for most parts of the world, indicating meteorological nudging advances the simulated daily variations of most aerosol species. Focusing on the Saharan desert and the associated outflow regions where aerosols are generally dominated by dust aerosols, it is obvious the correlation coefficients over those areas are significantly increased with nudged NICAM. The Atlantic areas near by the Saharan desert where frequently affected by the transport of the Saharan dust generally have a larger increase of correlation coefficient than other ocean areas, indicating that meteorological nudging can improve the model capability to simulate both the daily variation of dust source and the transport of the Saharan dust. The AOD simulations over the East Asian dust source regions are slightly improved, indicating simulations of the East Asian dust processes, even with nudging technique, are still difficult.

3.5. Dust-aerosol direct radiative effect

To calculate the dust-aerosol DRE, the simulated dust mass concentrations are transferred to the NICAM radiative transfer module named "mstrnX" (Nakajima et al., 2000; Sekiguchi and Nakajima, 2008). The dust-aerosol DREs are diagnosed by calling the radiation scheme twice, with including aerosol radiative effects of all the simulated aerosol components (i.e., dust and non-mineral dust aerosols) in the first call and without including the dust aerosols in the second call. In such double-call simulations, meteorology remains the same independent of the aerosols included in the radiation calculation as same as Bellouin et al. (2011) except we also remain the same cloud effective sizes (after considering the aerosol first indirect effects) in the double-call simulations. Therefore, the differences of net irradiances between the double-call calculations represent only the dust DREs, and the aerosol radiative effects of all the simulated aerosol components are used to advance the model into its next time step. The estimated annual global mean dust-aerosol DREs of NDG_UVTQP in the shortwave spectrum in a cloud-free sky at the top of the atmosphere (TOA), surface, and within the atmosphere are −1.3, −1.8, and 0.5 Wm^{-2},

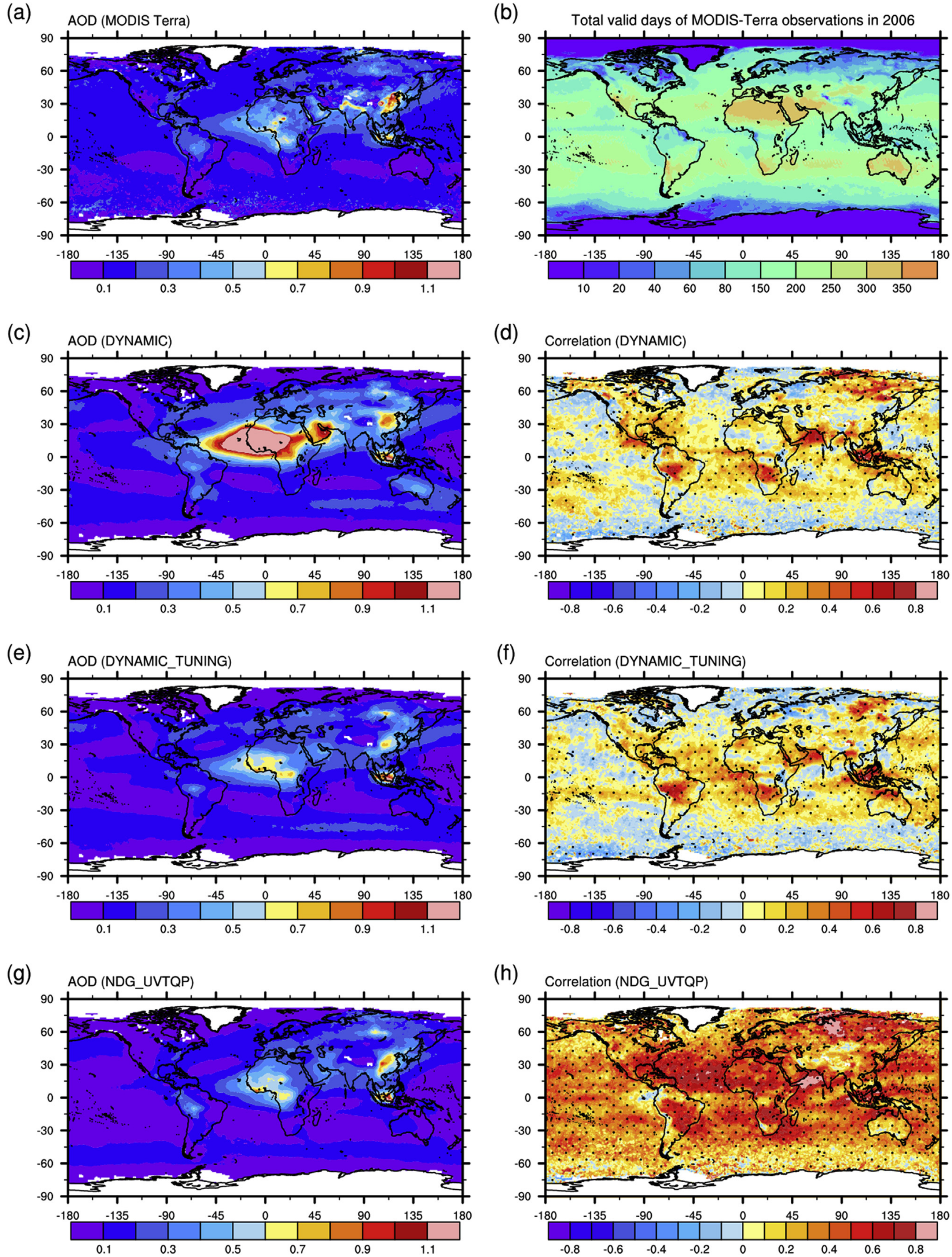

Fig. 11. The horizontal distributions of the annual mean AODs (a) and the total valid days (b) of MODIS-Terra Level 3 (L3) deep blue/dark target merged product in 2006. The horizontal distributions of the NICAM-simulated annual mean total AODs and the correlation coefficients of the modeled daily mean total AODs and the MODIS-Terra retrieved ones for DYNAMIC (c, d), DYNAMIC_TUNING (e, f), and NDG_UVTQP (g, h). The black dots indicate the points reaching and exceeding the 95% confidence level. (For interpretation of the references to color in this figure legend, the reader is referred to the Web version of this article.)

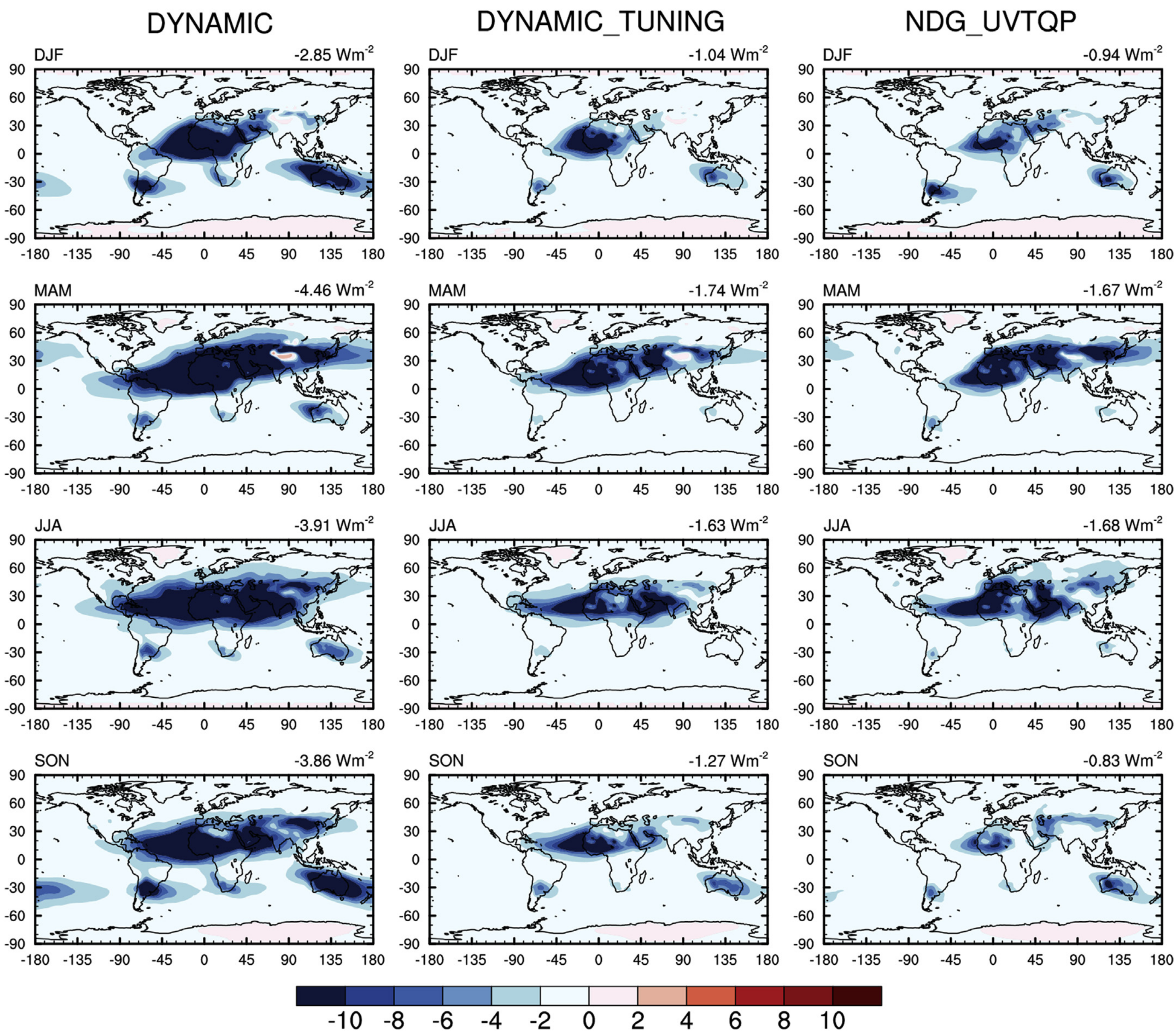

Fig. 12. The spatial distributions of the seasonal mean dust-aerosol DREs in a cloud-free sky at the top of the atmosphere.

respectively, which agree well with the corresponding values of −1.4, −1.9, and 0.5 Wm^{-2}, as estimated by the MACC reanalysis (Bellouin et al., 2013). The estimated DREs of DYNAMIC_TUNING are generally similar as the NDG_UVTQP with values of −1.4, −2.0, and 0.6 Wm^{-2}, respectively. The estimated DREs of DYNAMIC are −3.8, −5.4, and 1.7 Wm^{-2}, respectively, which, as expected, are approximately three times higher than those of DYNAMIC_TUNING, indicating that the DREs generally respond linearly to changes in the emission strengths of natural aerosol sources (Rap et al., 2013). The spatial distributions of the seasonal mean dust-aerosol DREs at the TOA are shown in Fig. 12. The DREs are clearly stronger over the Northern Hemisphere dust source and outflow regions in all the three experiments. The DREs of nudged NICAM reveal a more obvious seasonal variation, with larger values in the spring and summer and smaller values in the autumn and winter, which is generally consistent with the results of Bellouin et al. (2013). The DREs in the autumn of both the two dynamic experiments are comparable to those of the spring and summer due to the significant overestimation of the 10 m wind speeds and the associated dust emissions over the Sahara Desert region, as shown in Fig. 4.

4. Conclusions

In this study, we simulate and evaluate the dust cycles for present day conditions with a new dust-atmosphere model based on the NICAM coupled with the SPRINTARS. The effects of the meteorological nudging on the dust simulations are also investigated via running two versions of the model with and without constraining the wind (u, v), pressure (p), temperature (t), and the specific humidity (q_v) using the NCEP FNL reanalysis data. The dynamic NICAM tends to systematically overestimate the daily 10 m wind speeds over the two major desert regions (Saharan desert and East Asian desert) by approximately 30%–40%, whereas the meteorological nudging can obviously improve the capability of the model to simulate the daily 10 m wind speeds over the two major dust source regions, especially over the Saharan desert region. The estimated annual global mean dust emission flux with meteorological nudging is 1463 $Tg\,yr^{-1}$, which is generally consistent with the estimated emission fluxes for desert dust, as assimilated from observed AODs in a global aerosol model and the mean of the AeroCom models. There are significant responses of dust simulations to the overestimations of 10 m wind speeds in the dynamic version (e.g., the estimated annual global mean dust emission flux is 4.2 times higher than that of the nudged version), therefore, we cannot use the dust emission parameterizations with reanalysis winds and then use the same parameters with online winds to obtain a good simulation as also found in other dust model (Albani et al., 2014). It is found that the overestimations of the dust emissions are mainly caused by the overestimations of 10 m wind speeds especially over the Saharan desert where the soil moisture and snow amount are generally similar between the dynamic and nudged versions. Compared to the soil moisture and snow amount, the dust emissions have the highest relationships with the 10 m wind speeds over both the Saharan and East Asian deserts. The overestimations of 10 m winds are mainly caused by the positive biases of winds from surface to approximately 2 km and slightly affected by the temperatures. The winds only nudging can significantly reduce the overestimations of the 10 m winds, and the nudging of additional temperatures can further slightly improve 10 m winds. We therefore conclude the overestimations of 10 m winds are mainly caused by the positive biases of winds and slightly affected by the temperatures.

The evaluations of the simulated dust depositions and surface concentrations against the observations from the AeroCom benchmark dataset related to dust aerosols all show that meteorological nudging can improve the ability of the model to simulate the monthly variations in the dust depositions across the Atlantic and the surface dust concentrations across the Pacific. The daily variations in the simulated dust AODs are evaluated using the AERONET- and MODIS-retrieved daily AODs. A total of 2427 daily mean AODs over 31 AERONET "dusty" stations are selected for comparison. The result shows that nudging the meteorological fields can significantly improve the ability of NICAM to simulate the daily dust variations, increasing the correlation coefficients from around 0.15 to 0.50. The correlations between the simulated daily total AODs and the MODIS-retrieved ones are also significantly increased over the Saharan desert and outflow regions, with the inclusion of meteorological nudging. Although tuning the dust emission fluxes in the dynamical version can improve the global annual mean AOD to a reasonable value, the dust seasonal and daily variations show limited improvements. These results indicate that meteorological nudging is a simple assimilation technique that can facilitate a more straightforward simulation of the monthly and daily dust variations and the associated dust-aerosol DREs through improving both the dust sources and transports.

At the same time, we find that the global annual mean dust lifetime and dust size distribution are quite similar between the dynamic and nudged NICAM. Since dust lifetime and size distribution are two critical factors for estimating dust radiative effects (Kok, 2011; Timmreck and Schulz, 2004), the similar global annual mean dust lifetime and size distribution reveal meteorological nudging does not significantly affects our estimations of the global and annual mean dust DREs although it changes the spatial and seasonal distributions of DREs. With comparable dust emissions, the estimated annual global mean dust-aerosol DREs in the shortwave spectrum at the TOA are -1.4 and -1.3 Wm^{-2} by the dynamic and nudged NICAM, respectively. Therefore, we can use the dynamic model to understand climate-dust interactions and looking at past or future dust changes in a global and annual scale. Furthermore, we can improve the model performances for some applications to better simulate the daily, monthly, and seasonal dust variations with the implementation of meteorological nudging which probably cannot be achieved by just tuning the dust emission flux.

Acknowledgments

This study was financially supported by the National Natural Science Funds of China (41475031, 41571130024, 41605083, and 41590875), the Strategic Priority Research Program of the Chinese Academy of Sciences (XDA2006010302), the Open Fund by the Key Laboratory of Meteorological Disaster of the Ministry of Education (KLME1410), the Public Meteorology Special Foundation of MOST (GYHY201406023), and the National Key R&D Program of China (2016YFC0202001, 2017YFC0209803). Some of the authors were supported by the Global Environment Research and Technology Development Fund S-12 of MOEJ, the Japan Aerospace Exploration Agency (JAXA)/Earth Observation Priority Research, and the Grant-in-Aid for Young Scientist A (grant 17H04711) in Japan. The model simulations were performed using the supercomputer resources JAXA/JSS2, NIES/NEC SX-ACE, and PRIMEHPC FX10 (University of Tokyo, Japan). We are thankful to the researchers who provided the AeroCom (http://aerocom.met.no/), MODIS (https://modis-atmos.gsfc.nasa.gov/products/aerosol), AERONET (https://aeronet.gsfc.nasa.gov), and NCEP FNL reanalysis data. We also thank two anonymous reviewers for their insightful comments and suggestions.

References

Ackerley, D., Joshi, M.M., Highwood, E.J., Ryder, C.L., Harrison, M.A.J., Walters, D.N., Milton, S.F., Strachan, J., 2012. A comparison of two dust uplift schemes within the same general circulation model. Advances in Meteorology 2012, 1–13.

Albani, S., Mahowald, N.M., Perry, A.T., Scanza, R.A., Zender, C.S., Heavens, N.G., Maggi, V., Kok, J.F., Otto-Bliesner, B.L., 2014. Improved dust representation in the community atmosphere model. J. Adv. Model. Earth Syst. 6, 541–570.

Andreae, M.O., Charlson, R.J., Bruynseels, F., Storms, H., Grieken, R., Maenhaut, W., 1986. Internal mixture of sea salt, silicates, and excess sulfate in marine aerosols. Science 232, 1620–1623.

Arakawa, A., Schubert, W.H., 1974. Interaction of a cumulus cloud ensemble with the large-scale environment, Part I. J. Atmos. Sci. 31, 674–701.

Astitha, M., Lelieveld, J., Abdel Kader, M., Pozzer, A., de Meij, A., 2012. Parameterization of dust emissions in the global atmospheric chemistry-climate model EMAC: impact of nudging and soil properties. Atmos. Chem. Phys. 12, 11057–11083.

Bagnold, R., 1941. The Physics of Blown Sand and Desert Dunes. Methuen, London.

Bellouin, N., Quaas, J., Morcrette, J.J., Boucher, O., 2013. Estimates of aerosol radiative forcing from the MACC re-analysis. Atmos. Chem. Phys. 13, 2045–2062.

Bellouin, N., Rae, J., Jones, A., Johnson, C., Haywood, J., Boucher, O., 2011. Aerosol forcing in the climate model intercomparison project (CMIP5) simulations by HadGEM2-ES and the role of ammonium nitrate. J. Geophys. Res. 116 D20206.

Boylan, J.W., Russell, A.G., 2006. PM and light extinction model performance metrics, goals, and criteria for three-dimensional air quality models. Atmos. Environ. 40, 4946–4959.

Chen, S., Huang, J., Qian, Y., Zhao, C., Kang, L., Yang, B., Wang, Y., Liu, Y., Yuan, T., Wang, T., Ma, X., Zhang, G., 2017. An overview of mineral dust modeling over East Asia. Journal of Meteorological Research 31, 633–653.

Chin, M., Diehl, T., Dubovik, O., Eck, T., Holben, B., Sinyuk, A., Streets, D., 2009. Light absorption by pollution, dust, and biomass burning aerosols: a global model study and evaluation with AERONET measurements. Ann. Geophys.: atmospheres, hydrospheres and space sciences 27, 3439–3464.

Colarco, P., da Silva, A., Chin, M., Diehl, T., 2010. Online simulations of global aerosol distributions in the NASA GEOS-4 model and comparisons to satellite and ground-based aerosol optical depth. J. Geophys. Res. 115, D14207.

Dai, T., Goto, D., Schutgens, N.A.J., Dong, X., Shi, G., Nakajima, T., 2014. Simulated aerosol key optical properties over global scale using an aerosol transport model coupled with a new type of dynamic core. Atmos. Environ. 82, 71–82.

Ginoux, P., Chin, M., Tegen, I., Prospero, M., Holben, B., Dubovik, O., Lin, S., 2001. Sources and distributions of dust aerosols simulated with the GOCART model. J. Geophys. Res. Atmos. 106 (D17), 20255–20273.

Ginoux, P., Prospero, J.M., Gill, T.E., Hsu, N.C., Zhao, M., 2012. Global-scale attribution of anthropogenic and natural dust sources and their emission rates based on MODIS Deep Blue aerosol products. Rev. Geophys. 50, RG3005.

Goto, D., Dai, T., Satoh, M., Tomita, H., Uchida, J., Misawa, S., Inoue, T., Tsuruta, H., Ueda, K., Ng, C.F.S., Takami, A., Sugimoto, N., Shimizu, A., Ohara, T., Nakajima, T., 2015. Application of a global nonhydrostatic model with a stretched-grid system to regional aerosol simulations around Japan. Geosci. Model Dev. (GMD) 8, 235–259.

Gyan, K., Henry, W., Lacaille, S., Laloo, A., Lamsee-Ebanks, C., McKay, S., Antoine, R.M., Monteil, M.A., 2005. African dust clouds are associated with increased paediatric asthma accident and emergency admissions on the Caribbean island of Trinidad. Int. J. Biometeorol. 49, 371–376.

Han, Y., Fang, X., Zhao, T., Bai, H., Kang, S., Song, L., 2009. Suppression of precipitation by dust particles originated in the Tibetan Plateau. Atmos. Environ. 43, 568–574.

Holben, B., Eck, T., Slutsker, I., Tanre, D., Buis, J., Setzer, A., Vermote, E., Reagan, J., Kaufman, Y., Nakajima, T., 1998. AERONET—a federated instrument network and data archive for aerosol characterization. Rem. Sens. Environ. 66, 1–16.

Hopcroft, P.O., Valdes, P.J., Woodward, S., Joshi, M.M., 2015. Last glacial maximum radiative forcing from mineral dust aerosols in an Earth system model. J. Geophys. Res.: Atmosphere 120, 8186–8205.

Huang, J., Lin, B., Minnis, P., Wang, T., Wang, X., Hu, Y., Yi, Y., Ayers, J.K., 2006a. Satellite-based assessment of possible dust aerosols semi-direct effect on cloud water path over East Asia. Geophys. Res. Lett. 33 L19802.

Huang, J., Minnis, P., Lin, B., Wang, T., Yi, Y., Hu, Y., Sun-Mack, S., Ayers, K., 2006b. Possible influences of Asian dust aerosols on cloud properties and radiative forcing observed from MODIS and CERES. Geophys. Res. Lett. 33 L06824.

Huneeus, N., Chevallier, F., Boucher, O., 2012. Estimating aerosol emissions by

assimilating observed aerosol optical depth in a global aerosol model. Atmos. Chem. Phys. 12, 4585–4606.
Huneeus, N., Schulz, M., Balkanski, Y., Griesfeller, J., Prospero, J., Kinne, S., Bauer, S., Boucher, O., Chin, M., Dentener, F., Diehl, T., Easter, R., Fillmore, D., Ghan, S., Ginoux, P., Grini, A., Horowitz, L., Koch, D., Krol, M.C., Landing, W., Liu, X., Mahowald, N., Miller, R., Morcrette, J.J., Myhre, G., Penner, J., Perlwitz, J., Stier, P., Takemura, T., Zender, C.S., 2011. Global dust model intercomparison in AeroCom phase I. Atmos. Chem. Phys. 11, 7781–7816.
Jiménez-Guerrero, P., Pérez, C., Jorba, O., Baldasano, J.M., 2008. Contribution of Saharan dust in an integrated air quality system and its on-line assessment. Geophys. Res. Lett. 35 L03814.
Joussaume, S., 1990. Three-dimensional simulations of the atmospheric cycle of desert dust particles using a general circulation model. J. Geophys. Res. Atmos. 95 (D2), 1909–1941.
Kienast, S.S., Winckler, G., Lippold, J., Albani, S., Mahowald, N.M., 2016. Tracing dust input to the global ocean using thorium isotopes in marine sediments: ThoroMap. Global Biogeochem. Cycles 30, 1526–1541.
Kinne, S., Schulz, M., Textor, C., Guibert, S., Balkanski, Y., Bauer, S.E., Berntsen, T., Berglen, T.F., Boucher, O., Chin, M., Collins, W., Dentener, F., Diehl, T., Easter, R., Feichter, J., Fillmore, D., Ghan, S., Ginoux, P., Gong, S., Grini, A., Hendricks, J., Herzog, M., Horowitz, L., Isaksen, I., Iversen, T., Kirkevag, A., Kloster, S., Koch, D., Kristjansson, J.E., Krol, M., 2006. An AeroCom initial assessment - optical properties in aerosol component modules of global models. Atmos. Chem. Phys. 6, 1815–1834.
Kohfeld, K., Harrison, S., 2001. DIRTMAP: the geological record of dust. Earth Sci. Rev. 54, 81–114.
Kok, J.F., 2011. A scaling theory for the size distribution of emitted dust aerosols suggests climate models underestimate the size of the global dust cycle. Proc. Natl. Acad. Sci. Unit. States Am. 108, 1016–1021.
Lamarque, J.F., Bond, T.C., Eyring, V., Granier, C., Heil, A., Klimont, Z., Lee, D., Liousse, C., Mieville, A., Owen, B., Schultz, M.G., Shindell, D., Smith, S.J., Stehfest, E., Van Aardenne, J., Cooper, O.R., Kainuma, M., Mahowald, N., McConnell, J.R., Naik, V., Riahi, K., van Vuuren, D.P., 2010. Historical (1850–2000) gridded anthropogenic and biomass burning emissions of reactive gases and aerosols: methodology and application. Atmos. Chem. Phys. 10, 7017–7039.
Le Trent, H., Li, Z.X., 1991. Sensitivity of an atmospheric general circulation model to prescribed SST changes: feedback effects associated with the simulation of cloud optical properties. Clim. Dynam. 5, 175–187.
Levy, R.C., Mattoo, S., Munchak, L.A., Remer, L.A., Sayer, A.M., Patadia, F., Hsu, N.C., 2013. The Collection 6 MODIS aerosol products over land and ocean. Atmospheric Measurement Techniques 6, 2989–3034.
Liu, X., Easter, R.C., Ghan, S.J., Zaveri, R., Rasch, P., Shi, X., Lamarque, J.F., Gettelman, A., Morrison, H., Vitt, F., Conley, A., Park, S., Neale, R., Hannay, C., Ekman, A.M.L., Hess, P., Mahowald, N., Collins, W., Iacono, M.J., Bretherton, C.S., Flanner, M.G., Mitchell, D., 2012a. Toward a minimal representation of aerosols in climate models: description and evaluation in the Community Atmosphere Model CAM5. Geosci. Model Dev. (GMD) 5, 709–739.
Liu, X., Shi, X., Zhang, K., Jensen, E.J., Gettelman, A., Barahona, D., Nenes, A., Lawson, P., 2012b. Sensitivity studies of dust ice nuclei effect on cirrus clouds with the Community Atmosphere Model CAM5. Atmos. Chem. Phys. 12, 12061–12079.
Luo, C., Mahowald Natalie, M., del Corral, J., 2003. Sensitivity study of meteorological parameters on mineral aerosol mobilization, transport, and distribution. J. Geophys. Res.: Atmosphere 108. https://doi.org/10.1029/2003JD003483.
Mahowald, N., Kohfeld, K., Hansson, M., Balkanski, Y., Harrison, S.P., Prentice, I.C., Schulz, M., Rodhe, H., 1999. Dust sources and deposition during the last glacial maximum and current climate: a comparison of model results with paleodata from ice cores and marine sediments. J. Geophys. Res.: Atmosphere 104, 15895–15916.
Mahowald, N., Engelstaedter, S., Luo, C., Sealy, A., Artaxo, P., Benitez-Nelson, C., Bonnet, S., Chen, Y., Chuang, P., Cohen, D., Dulac, F., Herut, B., Johansen, A., Kubilay, N., Losno, R., Maenhaut, W., Paytan, A., Prospero, J., Shank, L., Siefert, R., 2009. Atmospheric iron deposition: global distribution, variability, and human perturbations. Ann Rev Mar Sci 1, 245–278.
Mellor, G.L., Yamada, T., 1982. Development of a turbulence closure model for geophysical fluid problems. Rev. Geophys. Space Phys. 20, 851–875.
Miller, R., Tegen, I., Perlwitz, J., 2003. Surface radiative forcing by soil dust aerosols and the hydrologic cycle. J. Geophys. Res. Atmos. 109 (D4), 361–375.
Miura, H., Satoh, M., Nasuno, T., Noda, A.T., Oouchi, K., 2007. A Madden-Julian Oscillation event realistically simulated by a global cloud-resolving model. Science 318, 1763–1765.
Miyamoto, Y., Kajikawa, Y., Yoshida, R., Yamaura, T., Yashiro, H., Tomita, H., 2013. Deep moist atmospheric convection in a sub-kilometer global simulation. Geophys. Res. Lett. 40, 4922–4926.
Mukai, M., Nakajima, T., Takemura, T., 2004. A study of long-term trends in mineral dust aerosol distributions in Asia using a general circulation model. J. Geophys. Res.: Atmosphere 109, D19204.
Nakajima, T., Tsukamoto, M., Tsushima, Y., Numaguti, A., Kimura, T., 2000. Modeling of the radiative process in an atmospheric general circulation model. Appl. Optic. 39, 4869–4878.
Nakanishi, M., Niino, H., 2006. An improved Mellor-Yamada level-3 model: its numerical stability and application to a regional prediction of advection fog. Boundary-Layer Meteorol. 119, 397–407.
Niwa, Y., Tomita, H., Satoh, M., Imasu, R., 2011. A three-dimensional icosahedral grid advection scheme preserving monotonicity and consistency with continuity for atmospheric tracer transport. J. Meteorol. Soc. Jpn. 89, 255–268.
NOAA/NCEP, 2000. NCEP FNL Operational Model Global Tropospheric Analyses, Continuing from July 1999 (Updated Daily). National Center for Atmospheric Research Computational and Information Systems Laboratory Research Data Archive. https://rda.ucar.edu/datasets/ds083.2/, Accessed date: 10 June 2017.
Noda, A.T., Oouchi, K., Satoh, M., Tomita, H., Iga, S., Tsushima, Y., 2010. Importance of the subgrid-scale turbulent moist process: cloud distribution in global cloud-resolving simulatioins. Atmos. Res. 96, 208–217.
Pan, D.M., Randall, D.D.A., 1998. A cumulus parameterization with a prognostic closure. Q. J. R. Meteorol. Soc. 124, 949–981.
Peng, Y., von Salzen, K., Li, J., 2012. Simulation of mineral dust aerosol with piecewise log-normal approximation (PLA) in CanAM4-PAM. Atmos. Chem. Phys. 12, 6891–6914.
Prospero, J., 1999. Long-term measurements of the transport of African mineral dust to the southeastern United States: implications for regional air quality. J. Geophys. Res.: Atmosphere 104, 15917–15927.
Prospero, J.M., Landing, W.M., Schulz, M., 2010. African dust deposition to Florida: temporal and spatial variability and comparisons to models. J. Geophys. Res. 115, D13304.
Prospero, J., Uematsu, M., Savoie, D.L., 1989. In: Riley, J.P. (Ed.), Mineral Aerosol Transport to the Pacific Ocean. Academic Press, New York, pp. 187–218 1989.
Rap, A., Scott, C.E., Spracklen, D.V., Bellouin, N., Forster, P.M., Carslaw, K.S., Schmidt, A., Mann, G., 2013. Natural aerosol direct and indirect radiative effects. Geophys. Res. Lett. 40, 3297–3301.
Remer, L.A., Kaufman, Y.J., Tanré, D., Mattoo, S., Chu, D.A., Martins, J.V., Li, R.R., Ichoku, C., Levy, R.C., Kleidman, R.G., Eck, T.F., Vermote, E., Holben, B.N., 2005. The MODIS aerosol algorithm, products, and validation. J. Atmos. Sci. 62, 947–973.
Ridgwell, A.J., 2002. Dust in the Earth system:The biogeochemical linking of land, air, and sea. Phil. Trans. 360 (1801), 2905–2924.
Ridley, D.A., Heald, C.L., Ford, B., 2012. North African dust export and deposition: a satellite and model perspective. J. Geophys. Res. 117 D02202.
Sato, Y., Goto, D., Michibata, T., Suzuki, K., Takemura, T., Tomita, H., Nakajima, T., 2018. Aerosol effects on cloud water amounts were successfully simulated by a global cloud-system resolving model. Nat. Commun. 9, 985.
Satoh, M., Matsuno, T., Tomita, H., Miura, H., Nasuno, T., Iga, S., 2008. Nonhydrostatic icosahedral atmospheric model (NICAM) for global cloud resolving simulations. J. Comput. Phys. 227, 3486–3514.
Satoh, M., Tomita, H., Yashiro, H., Miura, H., Kodama, C., Seiki, T., Noda, A.T., Yamada, Y., Goto, D., Sawada, M., Miyoshi, T., Niwa, Y., Hara, M., Ohno, T., Iga, S.-i., Arakawa, T., Inoue, T., Kubokawa, H., 2014. The non-hydrostatic icosahedral atmospheric model: description and development. Progress in Earth and Planetary Science 1 (18). http://www.progearthplanetsci.com/content/1/1/18.
Sayer, A.M., Hsu, N.C., Bettenhausen, C., Jeong, M.J., 2013. Validation and uncertainty estimates for MODIS Collection 6 “Deep Blue” aerosol data. J. Geophys. Res.: Atmosphere 118, 7864–7872.
Schutgens, N., Tsyro, S., Gryspeerdt, E., Goto, D., Weigum, N., Schulz, M., Stier, P., 2017. On the spatio-temporal representativeness of observations. Atmos. Chem. Phys. 17, 9761–9780.
Sekiguchi, M., Nakajima, T., 2008. A k-distribution-based radiation code and its computational optimization for an atmospheric general circulation model. J. Quant. Spectrosc. Radiat. Transf. 109, 2779–2793.
Smith, M.B., Mahowald, N.M., Albani, S., Perry, A., Losno, R., Qu, Z., Marticorena, B., Ridley, D.A., Heald, C.L., 2017. Sensitivity of the interannual variability of mineral aerosol simulations to meteorological forcing dataset. Atmos. Chem. Phys. 17, 3253–3278.
Sokolik, I.N., Winker, D.M., Bergametti, G., Gillette, D.A., Carmichael, G., Kaufman, Y.J., Gomes, L., Schuetz, L., Penner, J.E., 2001. Introduction to special section: outstanding problems in quantifying the radiative impacts of mineral dust. J. Geophys. Res.: Atmosphere 106, 18015–18027.
Stauffer, D.R., Seaman, N.L., 1990. Use of four-dimensional data assimilation in a limited-area mesoscale model. Part I: experiments with synoptic-scale data. Mon. Weather Rev. 118, 1250–1277.
Sudo, K., Takahashi, M., Kurokawa, J.I., Akimoto, H., 2002. CHASER: a global chemical model of the troposphere 1. Model description. J. Geophys. Res. 107. https://doi.org/10.1029/2001JD001113.
Suzuki, K., Nakajima, T., Numaguti, A., Takemura, T., Kawamoto, K., Higurashi, A., 2004. A study of the aerosol effect on a cloud field with simultaneous use of GCM modeling and satellite observation. J. Atmos. Sci. 61, 179–194.
Suzuki, K., Nakajima, T., Satoh, M., Tomita, H., Takemura, T., Nakajima, T.Y., Stephens, G.L., 2008. Global cloud-system-resolving simulation of aerosol effect on warm clouds. Geophys. Res. Lett. 35 L19817.
Takata, K., Emori, S., Watanabe, T., 2003. Development of the minimal advanced treatments of surface interaction and runoff. Global Planet. Change 38, 209–222.
Takemura, T., Egashira, M., Matsuzawa, K., Ichijo, H., O'Ishi, R., Abe-Ouchi, A., 2009. A simulation of the global distribution and radiative forcing of soil dust aerosols at the Last Glacial Maximum. Atmos. Chem. Phys. 9, 3061–3073.
Takemura, T., Nozawa, T., Emori, S., Nakajima, T.Y., Nakajima, T., 2005. Simulation of climate response to aerosol direct and indirect effects with aerosol transport-radiation model. J. Geophys. Res. 110 D02202.
Takemura, T., Okamoto, H., Maruyama, Y., Numaguti, A., Higurashi, A., Nakajima, T., 2000. Global three-dimensional simulation of aerosol optical thickness distribution of various origins. J. Geophys. Res. 105, 17853–17873.
Tanaka, T.Y., Sekiyama, T.T., Maki, T., Mikami, M., 2011. The effects of snow cover and soil moisture on asian dust: I. A numerical sensitivity study. SOLA 7A, 36–39.
Tegen, I., 2003. Modeling the mineral dust aerosol cycle in the climate system. Quat. Sci. Rev. 22, 1821–1834.
Tegen, I., Fung, I., 1994. Modeling of mineral dust in the atmosphere sources, transport, and optical thickness. J. Geophys. Res. Atmos. 99 (D11), 22897–22914.
Textor, C., Schulz, M., Guibert, S., Kinne, S., Balkanski, Y., Bauer, S., Berntsen, T., Berglen, T., Boucher, O., Chin, M., Dentener, F., Diehl, T., Easter, R., Feichter, H.,

Fillmore, D., Ghan, S., Ginoux, P., Gong, S., Grini, A., Hendricks, J., Horowitz, L., Huang, P., Isaksen, I., Iversen, I., Kloster, S., Koch, D., Kirkevåg, A., Kristjansson, J.E., Krol, M., Lauer, A., Lamarque, J.F., Liu, X., Montanaro, V., Myhre, G., Penner, J., Pitari, G., Reddy, S., Seland, Ø., Stier, P., Takemura, T., Tie, X., 2006. Analysis and quantification of the diversities of aerosol life cycles within AeroCom. Atmos. Chem. Phys. 6, 1777–1813.

Timmreck, C., Schulz, M., 2004. Significant dust simulation differences in nudged and climatological operation mode of the AGCM ECHAM. J. Geophys. Res.: Atmosphere 109. https://doi.org/10.1029/2003JD004381.

Tomita, H., 2008. A stretched icosahedral grid by a new grid transformation. J. Meteorol. Soc. Jpn. 86A, 107–119.

Tomita, H., Satoh, M., 2004. A new dynamical framework of nonhydrostatic global model using the icosahedral grid. Fluid Dynam. Res. 34, 357–400.

Twohy, C.H., Kreidenweis, S.M., Eidhammer, T., Browell, E.V., Heymsfield, A.J., Bansemer, A.R., Anderson, B.E., Chen, G., Ismail, S., DeMott, P.J., Van Den Heever, S.C., 2009. Saharan dust particles nucleate droplets in eastern Atlantic clouds. Geophys. Res. Lett. 36 L01807.

Woodward, S., 2001. Modeling the atmospheric life cycle and radiative impact of mineral dust in the Hadley Centre climate model. J. Geophys. Res.: Atmosphere 106, 18155–18166.

Wu, C., Lin, Z., He, J., Zhang, M., Liu, X., Zhang, R., Brown, H., 2016. A process-oriented evaluation of dust emission parameterizations in CESM: simulation of a typical severe dust storm in East Asia. J. Adv. Model. Earth Syst. 8, 1432–1452.

Wu, C., Liu, X., Lin, Z., Rahimi-Esfarjani, S.R., Lu, Z., 2018a. Impacts of absorbing aerosol deposition on snowpack and hydrologic cycle in the Rocky Mountain region based on variable-resolution CESM (VR-CESM) simulations. Atmos. Chem. Phys. 18, 511–533.

Wu, M., Liu, X., Zhang, L., Wu, C., Lu, Z., Ma, P.L., Wang, H., Tilmes, S., Mahowald, N., Matsui, H., Easter Richard, C., 2018b. Impacts of aerosol dry deposition on black carbon spatial distributions and radiative effects in the community atmosphere model CAM5. J. Adv. Model. Earth Syst. 10. https://doi.org/10.1029/2017MS001219.

Yin, Y., Chen, L., 2007. The effects of heating by transported dust layers on cloud and precipitation: a numerical study. Atmos. Chem. Phys. 7, 3497–3505.

Yoshioka, M., Mahowald, N.M., Conley, A.J., Collins, W.D., Fillmore, D.W., Zender, C.S., 2007. Impact of desert dust radiative forcing on sahel precipitation: relative importance of dust compared to sea surface temperature variations, vegetation changes, and greenhouse gas warming. J. Clim. 20 (8), 1445–1467.

Yue, X., Wang, H., Liao, H., Fan, K., 2010. Simulation of dust aerosol radiative feedback using the GMOD: 2. Dust-climate interactions. J. Geophys. Res. 115 D04201.

Yue, X., Wang, H., Wang, Z., Fan, K., 2009. Simulation of dust aerosol radiative feedback using the Global Transport Model of Dust: 1. Dust cycle and validation. J. Geophys. Res. 114, D10202.

Zhang, K., Wan, H., Liu, X., Ghan, S.J., Kooperman, G.J., Ma, P.L., Rasch, P.J., Neubauer, D., Lohmann, U., 2014. Technical Note: on the use of nudging for aerosol–climate model intercomparison studies. Atmos. Chem. Phys. 14, 8631–8645.